CHARACTERISTICS OF MICRO PLASMA JET IN SEM AND ITS APPLICATIONS

Khanit Matra

A Dissertation Submitted to

Kochi University of Technology

in Partial Fulfillment of the Requirements

for the Degree of

Doctor of Philosophy in Electronic and Photonic Systems Engineering

Graduate School of Engineering

Kochi University of Technology

Kochi, Japan

September, 2013

ABSTRACT

This research proposes a DC gas discharge operated in a micro gas jet, and injected into an electron microscope chamber. Gas was injected through a few 20-50Ø μm orifice gas nozzle (OGN), and was evacuated by an additional pump in order to keep the high vacuum environment. Gas discharge was then ignited between the OGN anode and a counter electrode Silicon (Si) wafer. There were two discharge modes that were observed by the oscilloscope during experiment: continuous discharge mode and self-pulsing discharge mode. The characteristics of a real time plot of voltage and current during the self-pulsing discharge mode was investigated. The DC micro plasma jet was then subsequently applied for micro plasma processing—local sputter etching and local thin-film deposition. Thus, the characteristics of local sputter etching and thin-film deposition by micro plasma jet were studied. A local, hydrogenated amorphous carbon thin-film was deposited on the silicon wafer with a high deposition rate of Acetylene plasma (10 times higher than conventional PECVD); however, plasma could not be sustained for long operation time due to the deposition of the insulator thin-film covering the silicon cathode. A few 100Ø μm sputter etching area, dependent on the orifice hole size and gas profile, could be obtained with a high sputtering rate of Argon plasma, due to a higher current density (70mA/cm^2) compared to that of the conventional method by 35 times approximately.

ACKNOWLEDGMENTS

The author would like to express his profound gratitude to his advisor, Professor Akimitsu HATTA, for giving him the opportunity to pursue a doctoral degree in Kochi University of Technology. Thanks to Professor HATTA, the author has been receiving continuous encouragement and guidance during the conductance of his PhD. study in the Hatta-Furuta laboratory. Logical thinking and optimism during research are the things which Professor HATTA always teaches and emphasizes. The author also would like to express his gratitude to his co-adviser, Associate Professor Hiroshi FURUTA, for his help, friendly discussions, and valuable suggestions. Moreover, the author also would like to express his appreciation to the committee consisting of Professor Masaru SANADA, Professor Furuta MAMORU, and Associate Professor Sadao MOMOTA, for their many useful comments and suggestions.

The author would like to thank his laboratory members of the Hatta-Furuta laboratory, especially, Dr. Jun-Seok OH, Mr. Xin LI, Mr. Yusuke MIZOBUCHI, Mr. Hirofumi KOJI, Mr. Kazuki SEKIYA, and Mr. Yosuke MORI, for their help, encouragement, and friendship.

The author wishes to express his appreciation to Professor Lawrence Hunter and Assistant Professor Nantakan WONGKASEM (his former advisor at Khon Kaen University) for his encouragement during his study at Kochi University of Technology. The author also would like to thank Mikiko BAN Sensei, Mariko KUBO Sensei, Ms. Rika FUJII, and all International Relation Center members for their administrative, Japanese language instructions, and Japanese cultural exchange activities.

The author also would like to acknowledge Ms. Monica NUTH, Ms. Michelle NOYES, and Mr. Piyapong JANMAIMOOL for correcting the English grammar in this dissertation out of their friendship and kindness, as well as Dr. Phaisarn Sudwilai for his

kind guidance in conducting experiments. The author is grateful to Kochi University of Technology and Rotary Yoneyama Memorial Foundation for providing him financial support; the Special Scholarship Program and Rotary Yoneyama scholarship respectively. Moreover, the author would like to thank all members of East Kochi Rotary Club, especially Mr. Kenji URATA and his family. The author has been receiving their continuous merciful kindness and warmth.

The author would like to thank all of his friends in Thailand and Kochi for their friendship, support, and encouragement. Without them, the author's student life would not have been fulfilled. Moreover, the author wishes to express his appreciation to Thai people in Kochi, especially Dr. Narongpol DUMAVIBHAT and Ms. Tanitra JU-GNAM, for their precious friendship and continuous support. Thanks to Thai people in Kochi, the author feels like he has a second warm family here.

Last but not least, the author would love to thank and inform Mr. Visit SRISATHIT, his beloved grandfather in heaven, that his grandson has already succeeded the first stepping stone of his life. Moreover, the author would like to express his profound gratitude to his entire family member, Mrs. Vanlapa MATRA (mother), Mr.Thong-in MATRA (father), Mrs. La-ong SRISATHIT (grandmother), Mr. Patalapol MATRA (younger brother), and others. Without their warmth, care, love, and encouragement, the author would not have reached his goal. The author also would like to thank people whom he did not mention here; their support is also tremendously valuable to him. Thank you very much every one, the author really appreciates it.

みんなさん どうも ありがとうございました。

Khanit MATRA

2013

DEDICATION

The author wishes to dedicate this dissertation to his family and teachers

TABLE OF CONTENTS

List Of Figures

CHAPTER 1: GENERAL INTRODUCTION

1.1 GENERAL INTRODUCTION OF GAS DISCHARGE

In 1928, Plasma was first used to elucidate an ionized gas by the Nobel-Prize-winning American chemist Irving Langmuir [1.1]. Plasma is a Greek word, which means “moldable substance”. It was first originated to describe the fluid part of blood distinguished from the cellular components [1.2]. Plasma is assigned as a fourth state of matter due to its unique properties which are different from other three matters: solid, liquid and gas [1.3]. More than 95% of the matters in the universe consist of plasma; including, for example, the Sun, interstellar matter, planetary atmosphere, solar wind, lightning, and flames. Nowadays, plasma is utilized and applied in many ways of human life such as fluorescent lights, plasma television, arc welding, fabrication of electronic components, and medical treatment to name a few**.**

After neutral gas molecules are applied with a sufficiently high thermal energy or electric field, the gas will become ionized (called gas discharge or plasma). Plasma is characterized as the quasi neutrality consisting of a cloud of a balanced number of negatively-charged, positively-charged, and neutrally-charged particles as shown in figure 1.1 [1.4]. This means that inside the plasma is electrically neutral. Plasma exhibits a collective behavior, which means that the motion of charged particles inside plasma influences other particles’ motion; therefore, the charged particle will not show a single-particle motion. The collective behavior is due to the Coulomb forces created by the interaction of negative charges, positive charges, and neutral particles [1.4]. Due to this property, plasma will show collective electromagnetic effects. The collective behavior property is an important factor which distinguishes the plasma from solid, liquid and gas.

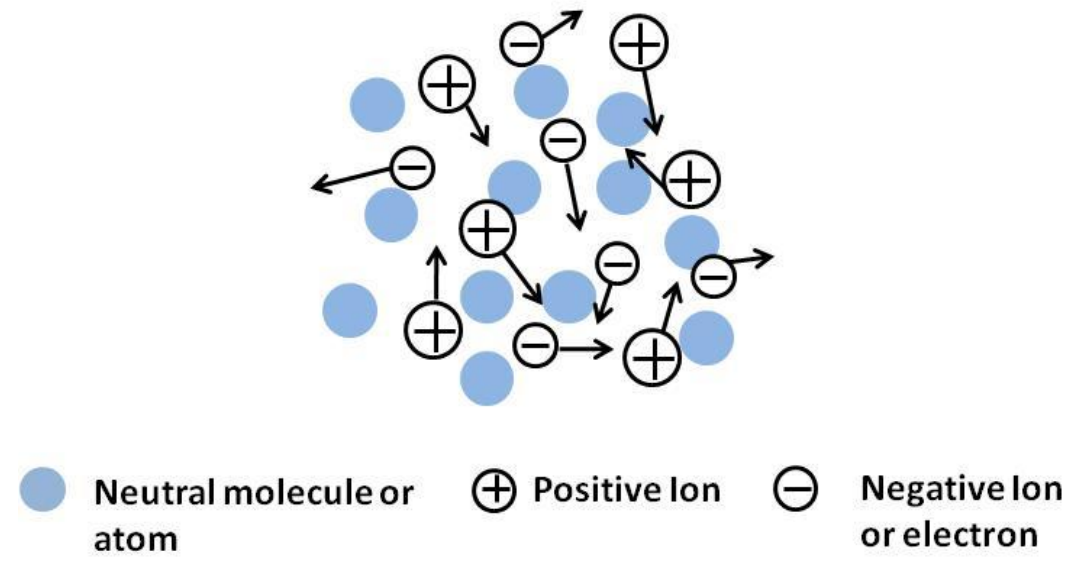

Figure 1.1 Charge compositions in plasma.

Since electron mass is very light (9.11×10^{-31} kilograms) compared to ion and neutral gas molecules [1.5]. Electrons are hence easy to be accelerated by external energy source compared to other particles. An electron, which has an energy of 1 eV (1.6 x 10^{-19}J), could have temperatures as high as 11605K [1.4]. Regarding the relative temperatures of the electrons (T_e), ions (T_i) and neutrals (T_g), plasma can be classified as "thermal" or "non-thermal". Thermal plasma (or equilibrium plasma), usually found at high pressures, has very effective energy exchange among electrons, ions, and neutral atoms due to the short mean free path, the high collision rate, and effective energy transfer. Therefore, in this condition, the temperature of electrons, ions, and neutral gas is almost the same ($T_e \approx T_i \approx T_g$) due to highly effective ionization, while non-thermal (or non-equilibrium plasma), usually found at low pressures, has a lower degree of ionization and lesser energy exchange efficiency compared to that of equilibrium plasma. Electrons in non-equilibrium plasma approach thermodynamic equilibrium much faster amongst electrons themselves, than they would exchanging energy with ions or neutral atoms [1.6]. For this reason, T_e may be very high and different from the average T_i and T_g ($T_e >> T_i > T_g$). In this work, only non-thermal atmospheric pressure plasma will be discussed. This

is due to the fact that the advantages of non-thermal atmospheric pressure plasma are merged from the good points of atmospheric pressure plasma and low pressure plasma. It offers non-equilibrium chemistry at high pressures with high ion, electron, and reactive specie densities, as well as high fluxes of photons [1.7].

1.2 RESEARCH BACKGROUND OF MICRO PLASMA

Recently, micro plasma has been paid much attention to because miniaturized size of various equipment types is required. Micro plasma is characterized as plasma of the small dimensions like its name [1.8]. Its size could be varied, ranging from tens to thousands of micrometers. Due to the various valuable properties of micro plasma, such as the ability to operate in atmospheric and sub-atmospheric pressure and to confine local plasma to less than micro scale, it's extremely attractive to many researchers' eyes. Moreover, its low operating cost, wide range of operating gas temperature (non-thermal and thermal plasma), and low power consumption make it attractive in many plasma applications [1.8-1.10]. These properties can be adjustable depending on material and geometry of the electrodes, gas type, operating gas pressure, and external power source for plasma generation. The flexibility of micro plasma production results in a wide range of applications such as sustainable energy, biomedical science, environmental science and many industrial fields [1.9].

(a)

(b)

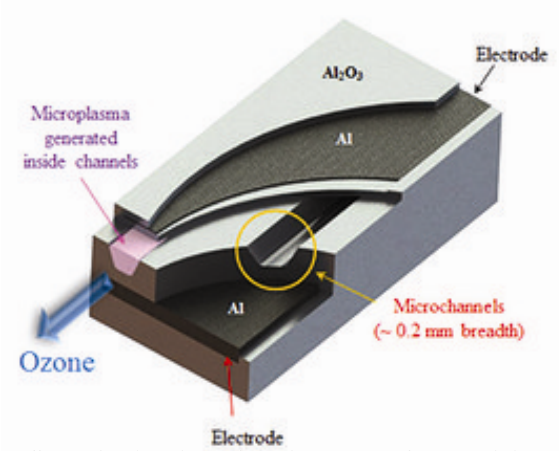

http://www.themicroplasmachannelsystems.com/?_escaped_fragment_=microplasma-technology/c6r8

(c)

Figure 1.2 Some applications of micro plasmas, (a) Plasma television, (b) Micro reactor for ozone generation and (c) Micro welding.

Figure 1.2 shows some applications of micro plasma in daily life. Plasma Display Panel (PDP) in figure 1.2a is a good example for micro plasma application in our daily life. In one plasma display panel, the panel is illuminated by many arrays of small pixels, in which each pixel is a micro plasma, similar to a tiny fluorescent lamp [1.11]. Due to the properties of micro plasma, the image quality could be enhanced and the angle of view could be widened [1.10]. Micro reactor for ozone generation in figure 1.2b is one interesting application in this era. The ozone layer in a high atmosphere could be converted from oxygen by the micro discharge channels consisted in a plasma reactor [1.12]. One application of high temperature plasma is welding. Micro welding shown in figure 1.2c is an effective tool in micro machining which is easy to handle and flexible to be used [1.13]. In the later part and entire of this thesis, the discussion is mainly focused on non-thermal micro plasma jet.

Non-thermal micro plasma jet is one of most famous micro plasma models. It is characterized as plasma bullets with flowing gas as depicted in figure 1.3 [1.14]. The plasma will be restricted in the dense gas flow boundary. Therefore, micro plasma jet is called a self-limited or space-limited discharge. Micro plasma jet had been first developed due to desired configuration for utilizing micro plasma as a radical or ion source which could be transported to a substrate directly and flexible to be used. Some configurations of micro plasma jet are micro hollow cathode, micro capillary discharge, and micro dielectric barrier plasma jet discharge.

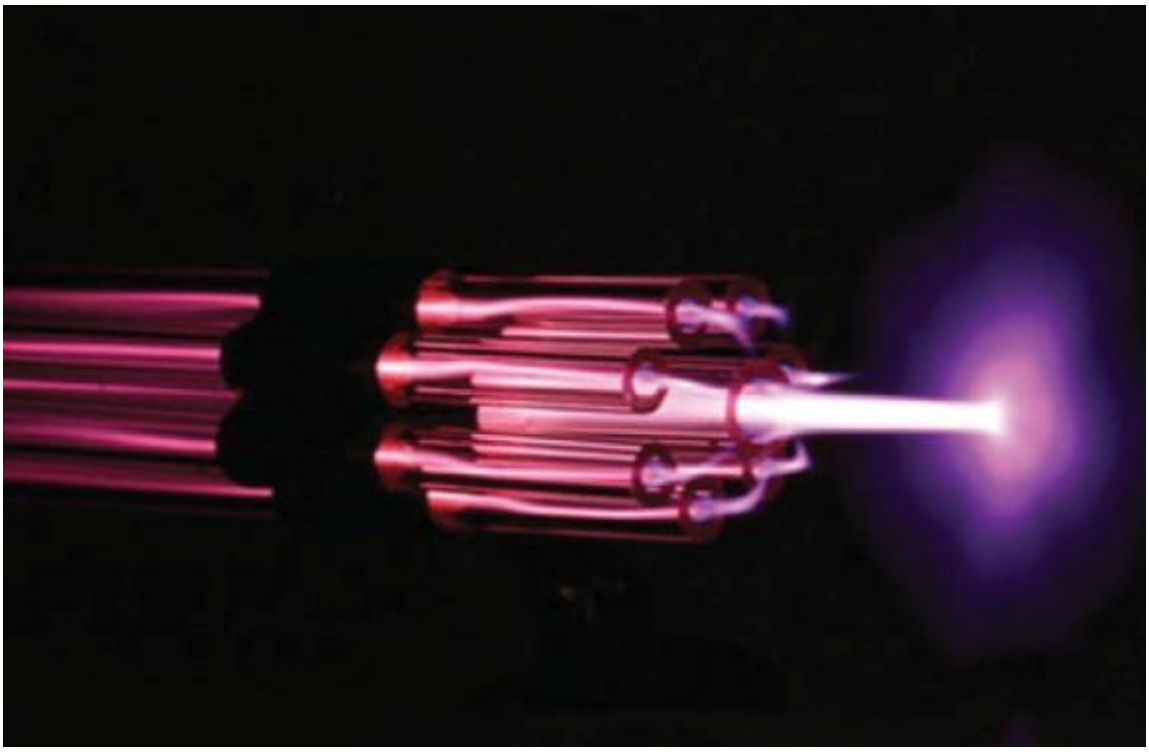

Figure 1.3 Micro plasma with flowing gas or micro plasma jet [1.14].

PROPERTIES AND APPLICATIONS OF MICRO PLASMA JET

Nowadays, the interest of micro plasma jet has been increased rapidly due to the requirements to reduce the plasma equipment cost and to improve the plasma equipment efficiency. Micro plasma jet has attracted much attention because of its various merits, such as its ability to confine micro scale local plasma generated in atmospheric and sub-atmospheric pressures [1.9, 1.15-1.16]. Moreover, possible non-thermal plasma generation, low power consumption, easy handling, and its low operating cost, since a high cost vacuum machine is not necessary, make it attractive in many plasma applications [1.8-1.16]. Some the important applications are mentioned as following:

1. Local surface modification

Regarding its high current density compared to its miniaturized plasma size, the high processing rate is possible; therefore, micro plasma is suitable for local surface modification which includes micro sputtering and micro deposition [1.17]. Moreover, since micro plasma is spatially controlled, a maskless patterning could be possible. Micro plasma is expected to play an important role in the microelectronics industry in the future, such as the micro fabrication and restoration of an integrated circuit (IC).

2. Micro reactor for nano particle growth

A geometry of the capillary shape electrode is not only suitable for supplying gas for plasma generation, but also is the micro reactor producer of various effective reactive species [1.17]. Since reactive species important in nano particle growth is directly transported through the gas flow, micro plasma jet could serve as the effective source for local nano particle synthesis. Moreover, micro plasma offers self-organization and bottom-up in nanofabrication mechanism [1.18]. The nano particles which have already been successfully fabricated by micro plasma jet are: diamonds [1.17-1.18], carbon nano sphere, and carbon nanotube [1.19]. In addition, this micro reactor is valuable for chemical analysis [1.20].

3. Biomedical and pollution treatment

As aforementioned that micro plasma jet is an effective reactor for reactive specie generation, micro plasma has already been applied in biomedical and pollution treatment recently. Since the plasma size could be controlled by experimental set up and geometry design, medical remedy for local treatment is possible without the deep impact on neighbor areas [1.21]. The ozone generation and waste water treatment could be achievable by micro plasma jet as well [1.22-1.23].

1.3 NOVELTY, OBJECTIVE, AND SCOPE IN THIS THESIS

CURRENT STATUS AND PROBLEM OF MICRO PLASMA

Nowadays, the electronic industry has been developing continuously. All electronic devices are aimed to be shrunk into a small size with higher efficiency. Therefore, comprehensive development is required for improving and generating a sensitive, reliable, and efficient portable device. Moreover, reducing operating cost is one important factor which is also considered. Due to the various advantages of micro plasma, such as high electron density, low power consumption, and miniaturized plasma size, it is an important factor which plays an essential role to propel not only the electronic industry but also other fields [1.6-1.10].

However, due to the small size of micro plasma, it causes a big problem and makes it difficult to study the micro plasma characteristics. Moreover, since the high pressure plasma has a high impact on the plasma, chemical reaction is complicated. Therefore, the atmospheric pressure plasma is rather different in contrast to low pressure plasmas and still only inadequately understood. Even though the micro plasma has already been studied for a hundred years, there are still many aspects of micro gas discharge phenomena which have not been clarified clearly yet. Henceforth, research on characteristics of micro plasma would open the window for a new aspect of micro gas discharge.

NOVELTY

DC micro plasma in scanning electron microscope (SEM) using small orifice gas nozzle (OGN) anode has been developed by our group [1.10, 1.24-1.26]. The usage of orifice type gas nozzle, consisting of a small hole on a thin wall, is a key issue for injection of localized high pressure micro gas jet into a vacuum environment. Otherwise, by using a micro capillary type gas nozzle, the pressure of injected gas becomes too small to operate gas discharge due to the poor conductance of long capillary tube.

Micro plasma processing in SEM is expected to be used for local restoration of micro electronics devices such as large-scaled integrated circuits (LSIs), fabrication of micro mechanical system devices (MEMS), and nanostructured material growth with SEM observation. In addition, there are advantages of plasma generation in SEM, such as the breakdown voltage of plasma ignition, which can be reduced by electron beam, and the profile of injected gas can be observed directly [1.26-1.27].

Because the injected gas rapidly disperses in the vacuum environment, the discharge gas locally exists at the exit of the OGN. The discharge space is limited in the dense gas jet area, whose profile is determined by the local high pressure gas injection and the rapid dispersion without any wall or any strict boundary. The micro gas jet in vacuum will bring some interesting features of not only the rapid gas flow but also the self-limited discharge space with a large gradient of pressure as compared to conventional gas discharge.

OBJECTIVE AND SCOPE OF THIS WORK

In this research, the aim of study is the characteristic of direct current (DC) gas discharge operated in a micro gas jet injected into a secondary electron microscope (SEM) chamber. A small OGN is adapted as an anode for use in localized micro plasma jet in SEM. The electrical characteristics of DC gas discharge operated in a micro gas jet injected in the SEM chamber will be clarified. The current and voltage characteristics are studied with variation of supplied pressure, electrode gap distance, and source voltage. Because the discharge current sometimes oscillates in a self-pulsating mode due to a large ballast resistance and a stray capacitance in the discharge circuit, the temporal wave forms of voltage and current are investigated by monitoring the digital oscilloscope.

The applications for DC micro plasma jet in SEM are aimed to apply in local micro plasma processing: local sputter etching and local thin-film deposition. The

characteristics of local sputter etching and thin-film deposition by micro plasma jet are aimed to clarify. Gap distance between the electrodes, gas flow rate supplied through the OGN, and discharge time and discharge current, playing an important role in the characteristics of local plasma processing, were optimized.

1.4 THESIS OUTLINE

The outlines of this thesis are constructed as followings:

Chapter 1: This chapter presents research background of micro plasma jet, novelty, objective, and scope of this thesis.

Chapter 2: The fundamental physics of gas discharge and its characteristics will be discussed.

Chapter 3: The experimental set up for the DC micro plasma jet performed in a vacuum environment will be presented. SEM and orifice gas nozzle which have played a crucial role in this research will be introduced.

Chapter 4: In this chapter, electrical characteristics of DC gas discharge operated in a micro gas jet injected in the SEM chamber are studied. The current and voltage characteristics were studied with variation of supplied pressure, electrode gap distance, and source voltage. The real time plots of voltage and current during pulsation will be investigated using a discharge model.

Chapter 5: After the characteristic of DC micro plasma jet operated inside SEM had already been studied, the application of this system will be applied in micro sputter etching for patterning on the silicon wafer in this chapter.

Chapter 6: In this chapter, micro plasma jet inside SEM will be applied in another application that is local thin-film deposition. The thin-film deposition and electrical

discharge characteristics were studied by varying electrode gap distance, discharge current, discharge voltage, and deposition time.

Chapter 7: Finally, the thesis conclusions will be summarized.

The outline chart of this thesis is illustrated in figure 1.4

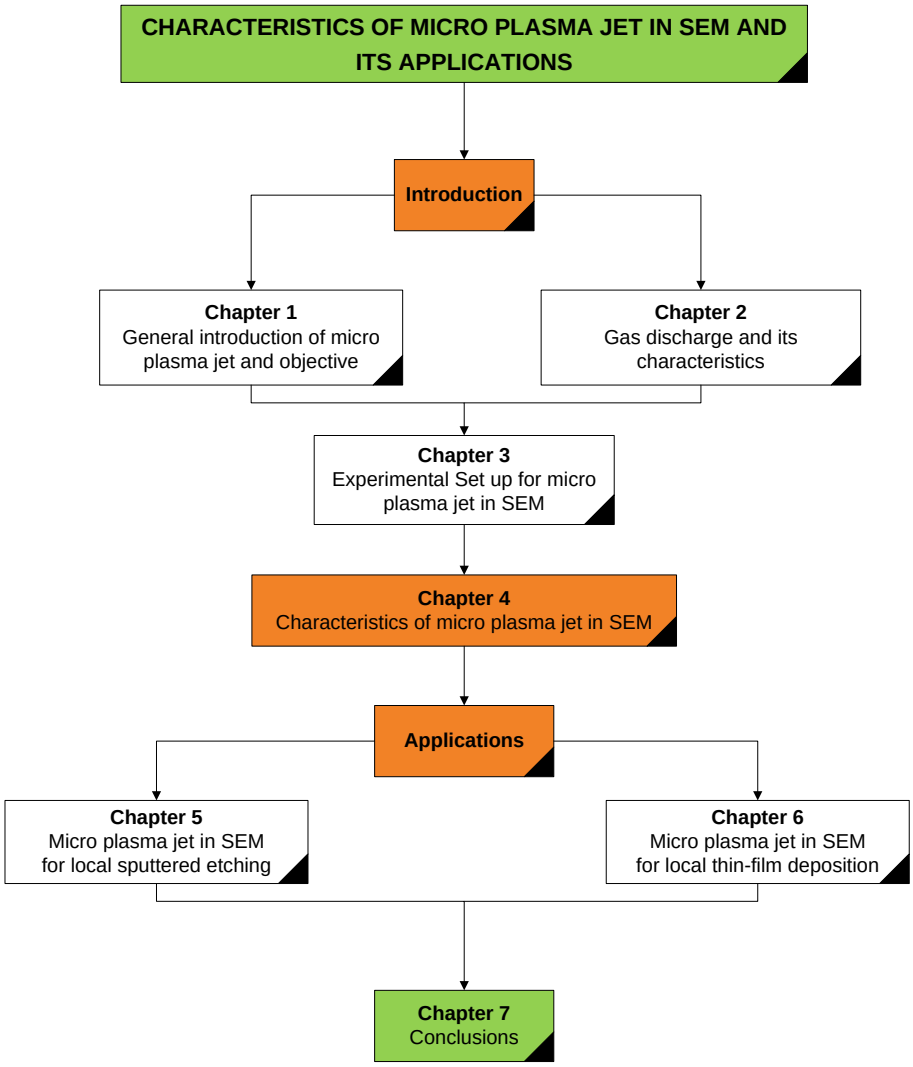

Figure 1.4 Outline chart of this thesis.

1.5 REFERENCES

[1.1] Braithwaite, R N Franklin and N St J. "80 Years Of Plasma." *Plasma Sources Science and Technology* 18.1 (2009): 010201.

[1.2] Anderson, S. (2007). *Collins dictionary*(9th ed.). Glasgow: HarperCollins.

[1.3] Chen, F. F., & Chang, J. P. (2003).*Lecture Notes on Principles of Plasma Processing*. Boston, MA: Springer US.

[1.4] Lieberman, M. A., & Lichtenberg, A. J. (1994). *Principles of plasma discharges and materials processing*. New York: Wiley.

[1.5] Brady, J. E., & Holum, J. R. (1988).*Fundamentals of chemistry* (3rd ed.). New York: Wiley.

[1.6] Sankaran, R. (2004). *HIGH-PRESSURE MICRODISCHARGES AS MICRO REACTORS FOR MATERIALS APPLICATIONS THESIS.pdf CALIFORNIA INSTITUTE OF TECHNOLOGY*. Ph.D. California institute of technology.

[1.7] Ellerweg, D. (2012). *Reaction chemistry in oxygen or hexamethyldisiloxane containing noble gas microplasma jets: a quantitative molecular beam mass spectrometry study*. Ph.D. Universität Bochum.

[1.8] Papadakis, A., Rossides, S., & Metaxas, A. (2011). Microplasmas: A Review. *Open Applied Physics Journal*, *4*, 45-63.

[1.9] Becker, K. H., Schoenbach, K. H., & Eden, J. G. (2006). Microplasmas And Applications. *Journal of Physics D: Applied Physics*, *39*(3), R55-R70.

[1.10] ZOU, Q. (2008). *MICROPLASMA PRODUCTION USING FIELD EMISSION CATHODE*. Ph.D. Kochi University of Technology.

[1.11] Tachibana, H., Ogawa, K., Nakajima, T., Nakagawa, T., Fujitani, M., & Sumida, K. (2008). Development Of 42-inch 1080p HD Plasma Display Panel. *The Journal of The Institute of Image Information and Television Engineers*, *62*(10), 1593-1597.

[1.12] Suzuki, S., & Sekiguchi, H. (2010). The Effect Of Catalytically Reactive Wall In A Micro-DBD Plasma Reactor On Ozone Decomposition. *Journal of Chemical Engineering of Japan*, *43*(2), 167-173.

[1.13] Tseng, K. H., Hsieh, S. T., & Tseng, C. C. (2003). Effect Of Process Parameters Of Micro-plasma Arc Welding On Morphology And Quality In Stainless Steel Edge Joint Welds. *Science and Technology of Welding & Joining*, *8*(6), 423-430.

[1.14] Kim, J. Y., Ballato, J., & Kim, S. (2012). Intense and Energetic Atmospheric Pressure Plasma Jet Arrays. *Plasma Processes and Polymers*, *9*(3), 253–260.

[1.15] Yoshiki, H. (2006). Generation of Air Microplasma Jet and Its Application To Local Etching Of Polyimide Films.*Japanese Journal of Applied Physics*, *45* (No. 6B), 5618-5623.

[1.16] Conrads, H., & Schmidt, M. (2000). Plasma generation and plasma sources.*Plasma Sources Science and Technology*,*9*, 441.

[1.17] Sankaran, R. M., & Giapis, K. P. (2002). Hollow Cathode Sustained Plasma Microjets: Characterization And Application to Diamond Deposition.*Journal of Applied Physics*, *92*(5), 2406.

[1.18] Sankaran, R. M., & Giapis, K. P. (2003). High-pressure Micro-discharges In Etching And Deposition Applications.*Journal of Physics D: Applied Physics*,*36*(23), 2914-2921.

[1.19] Yick, S., Han, Z., & Ostrikov, K. (2013). Atmospheric microplasma-functionalized 3D microfluidic strips within dense carbon nanotube arrays confine Au nanodots for SERS sensing. *Chem Commun (Camb)*,*49*(28), 2861-2863.

[1.20] Conrads, H., & Schmidt, M. (2000). Plasma generation and plasma sources.*Plasma Sources Science and Technology*,*9*, 441. [1.6]

[1.21] Fridman, A. A., & Friedman, G. (2013).*Plasma medicine*. Chichester, West Sussex, U.K.: John Wiley & Sons.

[1.22] Rani, D. A., Gomez, E., Boccaccini, A., Hao, L., Deegan, D., & Cheeseman, C. (2008). Plasma Treatment Of Air Pollution Control Residues. *Waste Management*, *28*(7), 1254-1262.

[1.23] Shimizu, K., Sugiyama, T., & Kanamori, M. (2008). Application of micro plasma for ozone generation and environmental Protection. *International Journal of Plasma Environmental Science and Technology*, *2*(1), 38-43.

[1.24] Zou, Q., Ishibashi, T., Ohi, H., Nakazawa, K., Kanakusa, H. and Hatta, A. (2006). Microplasma Discharge Using Carbon Nanotubes for Cathode. *ISDEIV' 06 International Symposium on Discharges and Electrical Insulation in Vacuum*, 2, 841-844.

[1.25] Ohi, H., Zou, Q. and Hatta, A., (2008). "Material Processing using Microplasma in SEM ", paper presented at *The 25th Symposium on Plasma Processing*, Yokohama. Yamacuchi, pp.111-112.

[1.26] Mizobuchi, Y., Fukunaga, K., Tojo, N., Tatsugawa, T., Sakai, T. and Hatta, A. (2009). "Discharge characteristics for micro-gas jet in vacuum", paper presented at *The 27th Symposium on Plasma Processing*, Yokohama, pp.113-115.

[1.27] Matra, K., Mitzobuchi, Y., Furuta, H. and Hatta, A. (2011). "Local sputtering by micro plasma jet in SEM", paper presented at *11th international symposium on Sputtering & Plasma Process*, Kyoto, pp. 46-49.

CHAPTER 2: GAS DISCHARGES

An artificial plasma or gas discharge could be generated by many methods such as DC (direct current) discharge, AC (Alternative current) discharge, RF (Radio frequency) discharge, microwave discharge, inductively and capacitively coupled discharges, and others [2.1]. However, the conventional gas discharge model is DC discharge, which has been studied for about hundred years. High DC voltage is not only the simplest method for gas discharge generation, but also suitable for micro plasma generation. This is due to the fact that the DC power source is easy to be scaled down to a size proper for the size of micro plasma model. Moreover, analysis of the DC system contains only a real number, thus the analysis would be simplified.

In this chapter, a brief introduction of micro DC gas discharge characteristics will be explained. Even though the characteristics of miniaturized DC gas discharge is much more complex than conventional DC gas discharge, many aspects of conventional DC gas discharge could be used as the assumptions for micro gas discharge clarification. Therefore, gas breakdown and its voltage current characteristics, and Paschen's law and the Similarity law, which are important keys for understanding micro gas discharge characteristics, are presented.

2.1 ELECTRICAL BREAKDOWN OF GAS

The condition which gas (an almost perfect insulator) becomes a conductor is called gas breakdown. Gas breakdown could happen when a sufficiently high potential power source is applied between two metal electrodes placed in a gas environment. A conventional DC glow discharge model was first proposed by William Crookes [2.2]. Figure 2.1 shows the conventional DC glow discharge in the vacuum tube. This model consists of two plane metal plates separated by a vacuum glass tube reactor filled with a few Argon gas pressure (13-1333 Pa) A ballast resistor used to limit the current flow in the circuit is placed between a DC power supply and an anode (a positively biased electrode).

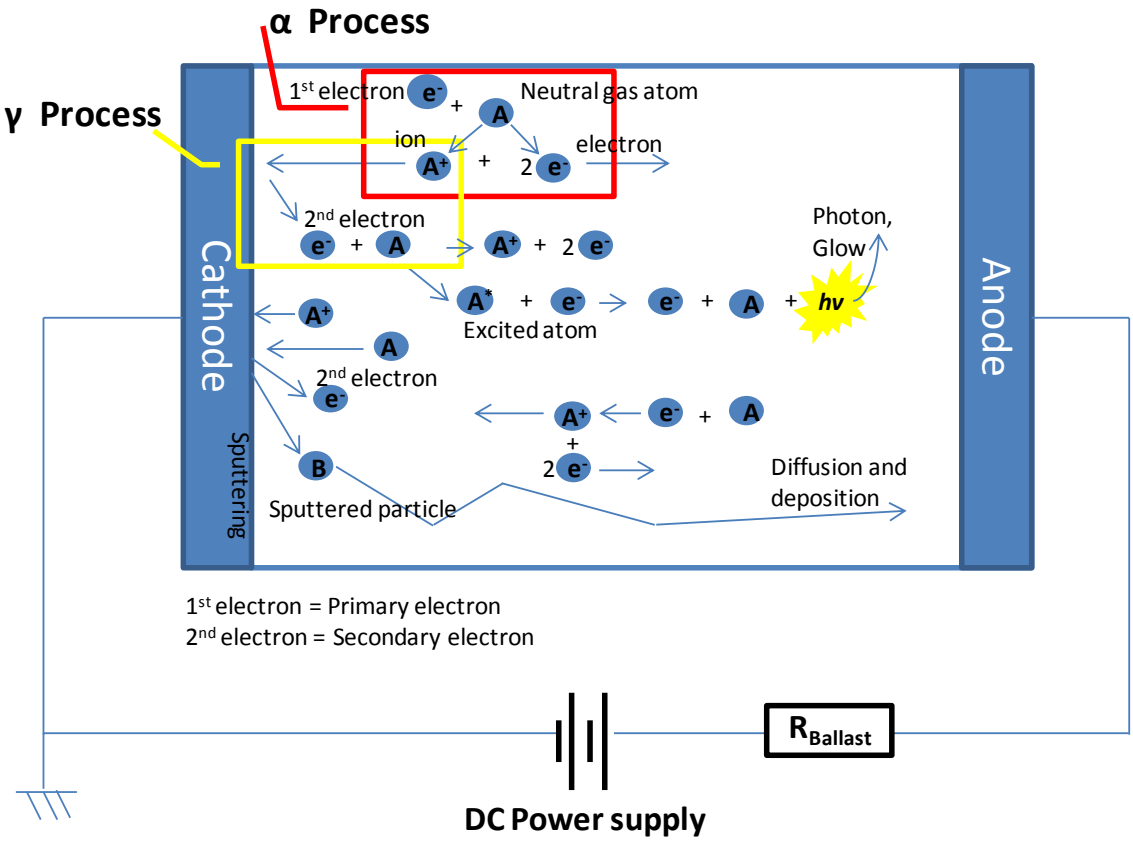

Figure 2.1 Schematic overview of a basic process in conventional DC glow discharge in the vacuum tube.

2.1.1 ELECTRON AVALANCHE MECHANISM (TOWNSEND BREAKDOWN PROCESS)

As the source voltage is slightly increased, a small amount of primary electrons or background electrons (e^-) from external source—such as cosmic rays, a nearby UV lamp and photo, field and thermionic emission from cathode—presented in the vacuum gas tube are accelerated to the anode. At the sufficiently high applied source voltage, the high energetic primary electrons may have more possibility to collide with other background atoms or molecules. The most important collision condition in gas breakdown is inelastic collision, resulting in ionization [$A + e^- \rightarrow A^+ + 2e^-$]; inelastic collision is the collision which causes non-conservative energy transfer during collision and excitation [$A + (e^- \text{ or } A \text{ or } A^+) \rightarrow A^* + (e^- \text{ or } A \text{ or } A^+)$; where A^* is an exited atom] [2.3]. However, excited atoms, ions, and electrons may also be de-excited or lessen their energy during the collision process as well. Primary electrons will transfer their energy to the neutral atoms via inelastic collisions. Some positive ions and electrons are created when electron inside neutral atom or molecule gains enough energy (higher than ionization energy) during collisions to free itself from neutral atom or molecule. The ionization due to electron is called electron impact ionization. At the small applied source voltage, the discharge needs external sources for the creation of electrons. The ionization may not happen, or happen very weakly. Therefore, this condition is called a *NON-SELF-SUSTAINING DISCHARGE*. This means the discharge will vanish when the electron source is removed. [2.4-2.5]

Assuming that one primary electron can cause one positive ion and one electron per one collision, there is a total of one positive ion and two electrons. Positive ions will travel towards the cathode side, while electrons will travel towards the anode side. The electrons may collide with other neutral atoms and cause a new ionization again. The cloud of positive ions and electrons created by this process is named electron avalanches. This multiplication of ions and electrons from primary electrons increased exponentially is known as α-process or primary ionization process. The electrons caused in this process will be denoted as α electron. [2.6]

α represents Townsend's first ionization coefficient. It is a number of average ionizing collisions caused by one primary electron per unit travelling from cathode to anode in the electric field. The flow of the electrons produced by ionization leads a current flowing in the circuit. The total current flow from this process could be calculated by

$$I = I_0 e^{\alpha d} \qquad (2.1)$$

Where I_0 is initial current flowing between electrodes caused by primary electrons, and d is the distance between the electrodes. The term $e^{\alpha d}$ is called the electron avalanche, and it is the number of electrons produced by one electron during travel from cathode to anode.

Due to the high electric field across anode and cathode, the positive ions (A^+) from α-process is accelerated towards, and hit, the metal plane cathode. Regarding the collision by energetic ions, electrons from metal plane cathode may be kicked off if the ion has energy higher than the work function of electrode material. The electron emitted from cathode, which is caused by the positive ions from α-process, is named secondary electron [2.7]. The secondary electron multiplication by ion bombardment at the cathode side is a secondary ionization process, γ-process, where γ is Townsend's secondary ionization coefficient. It is an average number of secondary electrons which are generated at the cathode per ionizing collision between the electrodes [2.6-2.7]. Therefore, the secondary electron could be denoted as γ electron. It should be noticed that in a DC gas discharge, the electrodes play an important role for sustaining plasma by secondary electron emission at the cathode side.

The γ electrons emitted from the cathode will be accelerated in electric field towards the anode side and serve as primary electrons for electron impact ionization in α-process. This electron multiplication is a cumulative process, which means that the number of free electrons from α-process and γ-process will be increased at the same time

as they are moving through the electric field. It could be seen clearly that α-process and γ-process have played a much crucial role in electron multiplication. Since the number of electrons created from α-process and γ-process is significantly increasing at the high applied source voltage, the electron avalanches hence have become high density, causing large current flowing in the circuit as well. If the increasing rate of current flowing in the circuit is satisfied as Townsend criteria in equation 2.2, a self-sustaining discharge could be established.

$$\gamma\,[\exp^{\alpha d}-1] = 1 \qquad (2.2)$$

The condition in which the gas discharge has satisfied the Townsend condition is called a *SELF-SUSTAINING DISCHARGE* or electrical breakdown of gas. The term 'self-sustaining discharge' means that the gas discharge itself does not need a supplying external primary electron for sustaining primary ionization. In the self-sustaining gas discharge mode, some excited atoms (A*) may release their energy by radiation in terms of photon, and turn back to the normal state during collision [A* → A + *hv* (photon)]. This process will cause the phenomenon called glow discharge, where the discharge becomes visible [2.4].

As aforementioned that in DC gas discharge, electrodes have played a crucial role to sustain self-sustaining discharge by secondary electron created at the cathode side, another important process existing at the cathode is sputtering. The metal atom from metal plane cathode will be kicked off or sputtered when energetic positive ions and fast neutral atoms from plasma hit the metal plane cathode, called sputtering. The sputtered atom will travel randomly and deposit on the anode side. Some of the sputtered atoms will diffuse out from the plasma and be deposited on the vacuum tube wall. Sometimes they are re-deposited on the cathode side [2.8].

Alternatively, not only electron multiplication caused by the ionization process, but also the electron loss due to the recombination process exists in the plasma.

Electron avalanche could be slowed down by the loss of electrons and electron energy losses. Electrons lose their energy after they collide with neutral atoms and molecules. Electrons also lose energy in the electric field by electron vibration and rotation, if they move against the drift direction after elastic collisions. Diffusion of drift electron during travel towards the anode leads to the removal of electrons from the field and out of the plasma boundary. Electrons could be loosed by attachment in electronegative gases as well. Therefore, to overcome the electron loose and maintain self-sustaining plasma, the electron multiplication process in plasma must be sufficient and effective [2.9].

2.1.2 PASCHEN'S LAW AND THE SIMILARITY LAW

By applying the Townsend criteria, it is possible to estimate the gas breakdown voltage (V_{BR}). For the uniform electric fields in a parallel-plate discharge condition, the electric field can be derived from the voltage divided by the gap distance,

$$E = V/d \tag{2.3}$$

Where E and V are electric field and voltage across the electrodes, while d is the distance between electrodes. Then, the equation 2.2 is rearranged into

$$d = \ln(1/\gamma + 1)/\alpha \tag{2.4}$$

To obtain the V_{BR}, the Townsend criterion in equation 2.4 is then substituted in equation 2.3. Therefore, V_{BR} can be rewritten as

$$V_{BR} = E.[\ln(1/\gamma + 1)]/\alpha \tag{2.5}$$

However, the terms of E and α have a relationship represented in equation 2.6

$$\alpha/\gamma = A.\exp(-Bp/E) \tag{2.6}$$

Where p is the gas pressure and the constants A and B are gas and electrode material-specific constant number, which are derived from experiments.

From equation 2.5 and 2.6, breakdown voltage, V_{BR}, could be therefore expressed as

$$V_{BR} = E.[Bpd / ln[Apd/(1/\gamma + 1)]] \qquad (2.7)$$

This equation is called Paschen's equation. It is named after Friedrich Paschen, a physicist who discovered it empirically in 1889 [2.10]. From Paschen's equation, it could be noticed that the breakdown voltage is dependent on the product of pd for a given gas and cathode material. Figure 2.2 presents Paschen's curve for V_{BR}, calculated by equation 2.7, at the different pd products of arbitrary gas between parallel plane metal electrodes.

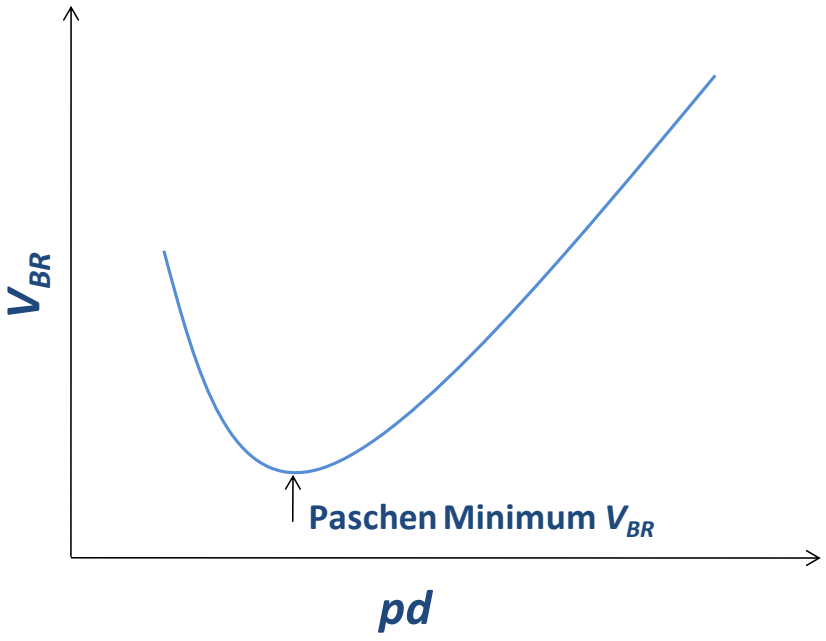

Figure 2.2 Paschen's curve for arbitrary gas between parallel plane metal electrodes.

By Paschen's equation, the minimum V_{BR} could be estimated at the intermediate *pd* product. Assume that the electrode gap distance is fixed at the constant value, and the pressure between the electrodes is increased from the left to the right-hand side of the x-axis of the Paschen's curve, thus the *pd* product is also increased from the left to the right-hand side of the Paschen's curve. Consider the left-hand side of minimum V_{BR} point, where V_{BR} is increasing rapidly since at the low pressure, it has a longer gas mean free path and very small gas density. This causes a very small possibility of collision. At the right-hand side of minimum V_{BR} point, V_{BR} is increasing slowly since at the high gas pressure, it has a shorter gas mean free path and high gas density leading to too high collision rate. Electrons which are travelling towards the anode have more frequent collisions with the neutral gas atoms or molecules. However, the energy which the neutral atoms receive during collisions is too small to cause ionization [2.5-2.10]. Therefore, to increase the probability of ionization, the high voltage applied to the system is required. However, the voltage increasing rate at the lower *pd* value is more rapid because in order to accelerate the electrons without or with few collisions across the gap, the gas discharge itself requires a numerous amount of external energy. However, it should be noticed that Paschen's curve for different gas and cathode material at the same *pd* values would have a similar curve shape; however, the curve would be shifted from the other conditions [2.4].

Regarding the Similarity laws [2.11] of classical theory, the voltage required to sustain the gas discharge at a certain discharge current is almost the same, if the ratio of electric field and pressure (E/p) is constant. Consequently, based on the fundamental knowledge of the Paschen's curve scaling and the Similarity laws, non-thermal atmospheric pressure glow discharge is achievable at the minimum V_{BR} by increasing the gas pressure (p) and decreasing the dimension of the device (d). Therefore, to operate plasma at a high pressure, miniaturized discharge dimensions is essential for plasma generation. It is expected that to operate plasma at atmospheric pressure, the *pd* values should be on the order of 10 Torr.cm [2.12-2.14].

2.2 VOLTAGE-CURRENT CHARACTERISTICS OF DC GAS DISCHARGE

In the previous section, the mechanisms of DC gas breakdown between metal parallel electrodes in the low vacuum tube have already been explained. However, there are many different discharge modes found in DC gas breakdown dependent on the discharge current. Regarding the voltage-current relationship, the DC discharge could be classified into 6 modes shown in figure 2.3 as following [2.4]:

1. Non-self sustaining discharge (A-B)

If a very small source voltage is applied between the electrodes, a small amount of background electrons presented in the vacuum gas tube are accelerated and swept to the anode causing an extremely small current flowing in the circuit (less than 10^{-10}A). The ionization of a neutral atom cannot happen due to too low applied source voltage. The applied source voltage is just for sweeping the background electrons towards the anode. If all background electrons have already arrived to the anode, there is no more current flow in the circuit. Therefore, this period is called *Non-Self Sustaining Discharge*, meaning the gas discharge could not be able to sustain without applied source voltage and primary electron source.

2. Townsend discharge (B-C)

The region after non-self sustaining discharge *is Townsend discharge*. In this mode, the applied source voltage is considerably increased compared to *Non-self sustaining discharge*, until the primary electrons can cause ionization of neutral gas atoms or molecules by electron impact. Therefore, this region is a transition region from non-self sustaining to *self-sustaining discharge*. When the electron multiplication process has satisfied the Townsend criteria, gas will be discharged. The voltage at the transition point is then called a breakdown voltage. However, the applied voltage value in this mode is slightly higher than the breakdown voltage; hence, the gas is very weakly ionized. Therefore, Townsend discharge is known as dark discharge since there is no light emission (photon, *hv*) from gas. Because the current rises considerably after gas

breakdown, even the source voltage is slightly increased; consequently, the *V-I* characteristic is almost slightly positively-sloped.

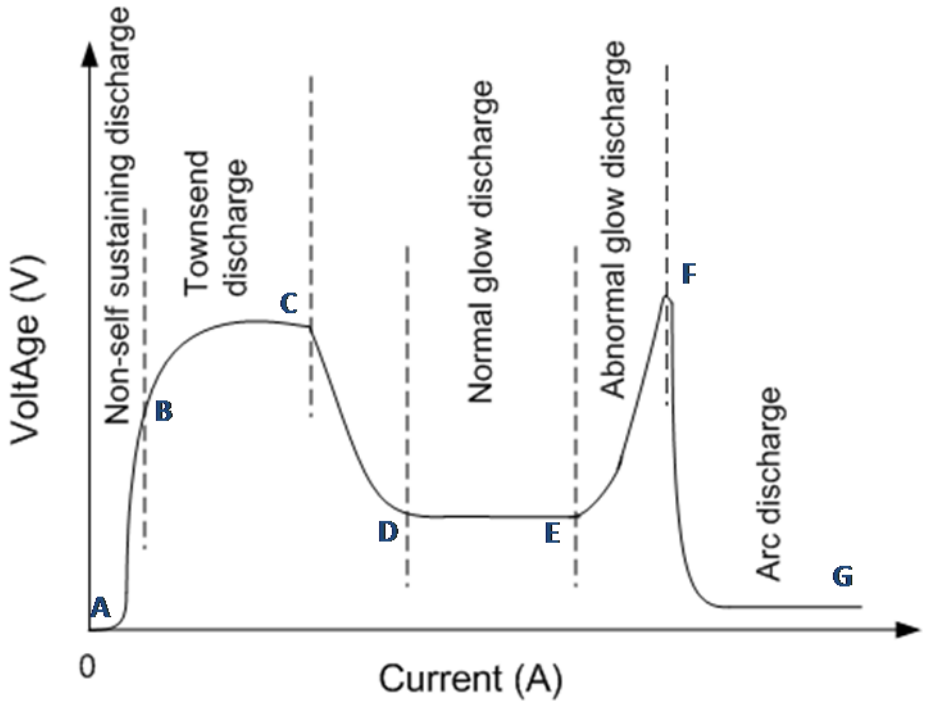

Figure 2.3 Voltage - current characteristics of DC gas discharge

3. Subnormal glow discharge (C-D)

Subnormal glow discharge is presented at the negative *V-I* slope in figure 2.3 after the Townsend discharge mode. This is due to the fact that increasing source voltage has played an important role in the high electron multiplication rate, leading to the space charge effect. After the neutral atoms are ionized, the electron avalanches rapidly travel towards the anode side. Compared to the positive ions, electrons have comparatively high mobility. Therefore, mainly the positive ions are left and concentrated in the front part of the cathode, called the cathode fall region. At the cathode fall region, there is a large voltage drop which is almost equal to applied source voltage

across the electrodes. Therefore, electron multiplication at the cathode fall region, due to increasing electric fields, is effectively increased. This effect allows the total voltage required to sustain the gas discharge to be reduced. Therefore, the *V-I* curve presents a negative slope of increasing discharge current. Due to the higher current flowing in this discharge mode compared to the Townsend discharge mode, the discharge becomes visible. Moreover, this discharge mode is rather unsteady and easily transitions to the next discharge mode; therefore, this discharge mode is called subnormal glow discharge.

4. Normal glow discharge (D-G)

A slightly further increase of applied source voltage completes the cathode fall region formation. The subnormal glow discharge then transitions to the normal glow discharge mode. At the beginning of this discharge mode, the plasma locally covers part of the cathode. Increasing the discharge current contributes to spreading the plasma, covering all the cathode area with a constant current density, the voltage thus remains almost constant. This phenomenon causes an almost flat *V-I* curve in the normal glow discharge. Most plasma processing is restricted in this normal glow discharge mode. This is because the gas discharge is operated at room temperature (non thermal plasma); moreover, the damage of electrodes could be preventable. In addition, the glow discharge can operate over a wide pressure regime.

5. Abnormal glow discharge (G-E)

After the whole cathode is fully covered by the plasma, a further increasing of current leads to an increase of the cathode fall region; therefore, voltage increases steeply. Since ions and electrons are accelerated by the application of a large source voltage in this discharge mode, ions and electrons will hit on the electrodes with high energy, raising the temperature of the cathode. Therefore, thermionic electron emission from the cathode begins to play a few roles in electron multiplication.

6. Arc discharge (E-F)

However, if the current is further increased, the cathode will be hit continually by the energetic ions. Therefore, the thermionic electron emission from the electrodes crucially affects the electron multiplications process. Regarding thermionic electron emission causing of a large current flow, the voltage required to sustain the discharge can be lowered significantly. The gas heating could be also happened in this discharge mode; therefore, the arc discharge mode is usually used in welding or engine propulsion.

2.3 MICRO GAS DISCHARGE AND MICRO PLASMA JET

2.3.1 MICRO GAS DISCHARGE

Non thermal atmospheric pressure plasma was developed because of the disadvantage of low pressure plasma operation; for example, high operating cost due to vacuum chamber, low ion, electron and reactive specie density, and difficulty to be integrated in production lines [2.1].

Regarding the Similarity laws [2.11] and Paschen's law, the first non-thermal atmospheric pressure micro plasma was proposed by Schoenbach et al. Micro hollow-cathode geometry was developed for micro plasma generation in the atmospheric environment. To generate non thermal atmospheric pressure plasma (760 Torr), the hollow cathode diameter needed to be shrunk down to 100–200 mm [2.14].

2.3.2 MICRO PLASMA JET

Even though atmospheric pressure plasmas can solve the disadvantages of low pressure plasma operation, it is difficult to sustain a glow discharge under the high pressure condition since the glow discharge easily transitions into arc discharge between the electrodes. Therefore, an atmospheric pressure micro plasma jet has been proposed to

help cool-the electrode temperature [2.14]. Moreover, micro plasma jet also has various advantages as mentioned in chapter one.

A conventional DC micro plasma jet configuration is demonstrated in figure 2.4. The model includes a capillary tube used to supply gas for plasma generation, a counter electrode, ballast resister used to limit the current flow in system and a power supply [2.16].

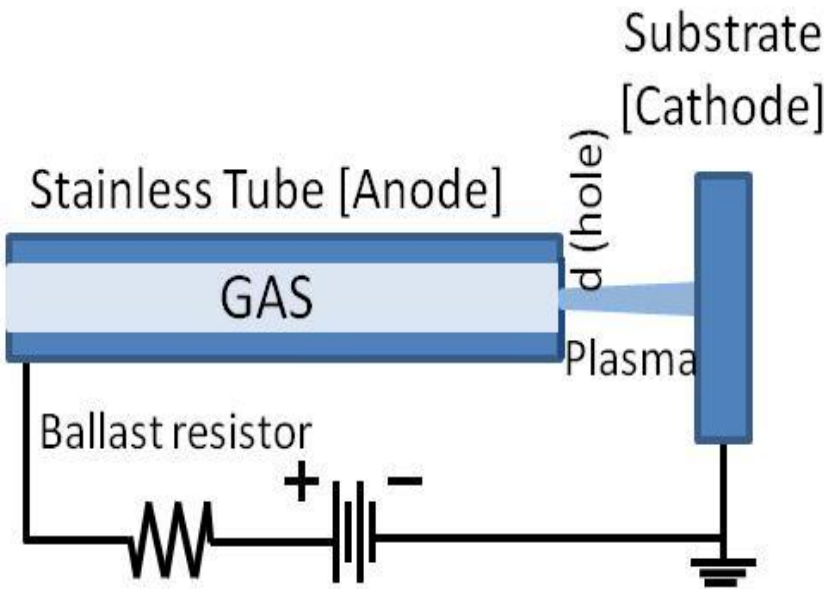

Figure 2.4 Schematic drawing of conventional DC Micro plasma jet

Even though the micro plasma jet model is considerably different from conventional DC gas discharge tube, because of its small dimension and non uniform gas pressure between electrodes due to rapid gas diffusion, some of its properties and characteristics could be explained based on a basic knowledge of conventional DC gas discharged between parallel electrodes in the vacuum tube [2.17, 2.18], presented in the previous sections.

In this research, a micro plasma jet was operated inside a vacuum chamber. As the gas jet is evacuated rapidly by the vacuum pump, the plasma characteristics will be different from conventional plasma jet system. The result is that the discharge space is limited by the dense gas jet area and the gas jet, evacuated by the vacuum pump, rapidly disperses without any wall or any strict boundary. The micro gas jet in vacuum creates some interesting features, not only the rapid gas flow but also the self-limited discharge space with a large gradient of pressure as compared to conventional gas discharge. Therefore, its characteristics need to be clarified. The plasma jet in this research is restricted by the power generated by DC power supply. This is due to the fact that the conventional DC gas discharge characteristics have already been well clarified; therefore, the characteristics of micro plasma jet operating in a vacuum environment could be simply clarified by comparing with the well-known discharge model.

2.4 REFERENCES

[2.1] Mitra, B. (2008). *DC PULSE-POWERED MICRODISCHARGES ON PLANAR ELECTRODES AND THEIR USE IN VAPOR AND LIQUID PHASE CHEMICAL SENSING IN AMBIENT AIR*. Ph.D. The University of Michigan.

[2.2] Lieberman, M. A., & Lichtenberg, A. J. (1994). *Principles of plasma discharges and materials processing*. New York: Wiley. [1.4]

[2.3] BOGAERTS, A. (1996). *Mathematical modeling of a direct current glow discharge in argon*. Ph.D. UNIVERSITAIRE INSTELLING ANTWERPEN.

[2.4] Wagenaars, E. (2006). *Plasma Breakdown of Low-Pressure Gas Discharges*. Ph.D. Technische Universiteit Eindhoven.

[2.5] Bogaerts, A., Neyts, E., Gijbels, R., & der Mullen, J. v. (2002). Gas Discharge Plasmas And Their Applications.*Spectrochimica Acta Part B: Atomic Spectroscopy*, *57*(4), 609-658.

[2.6] Breakdown of gaseous insulation. (n.d.).*Department of Electrical Engineering*. Retrieved July 18, 2013, from www.elect.mrt.ac.lk/HV_Chap1.pdf

[2.7] Christophorou, L. G. (1978). *High voltage research (breakdown strengths of gaseous and liquid insulators)*. Oak Ridge, Tenn.: Dept. of Energy, Oak Ridge National Laboratory.

[2.8] Chapman, B. N. (1980). *Glow discharge processes: sputtering and plasma etching*. New York: Wiley.

[2.9] ZOU, Q. (2008). *MICROPLASMA PRODUCTION USING FIELD EMISSION CATHODE*. Ph.D. Kochi University of Technology. [1.10]

[2.10] Paschen, F. (1889). Ueber Die Zum Funkenübergang In Luft, Wasserstoff Und Kohlensäure Bei Verschiedenen Drucken Erforderliche Potentialdifferenz. *Annalen der Physik*, *273*(5), 69-96.

[2.11] Sturges, D. J., & Oskam, H. J. (1964). Studies Of The Properties Of The Hollow Cathode Glow Discharge In Helium And Neon. *Journal of Applied Physics*, *35*(10), 2887.

[2.12] Iza, F., Kim, G. J., Lee, S. M., Lee, J. K., Walsh, J. L., Zhang, Y. T., et al. (2008). Microplasmas: Sources, Particle Kinetics, And Biomedical Applications. *Plasma Processes and Polymers*, *5*(4), 322-344.

[2.13] Foest, R., Schmidt, M., & Becker, K. (2006). Microplasmas, An Emerging Field Of Low-temperature Plasma Science And Technology. *International Journal of Mass Spectrometry*, *248*(3), 87-102.

[2.14] Schoenbach, K. H., Verhappen, R., Tessnow, T., Peterkin, F. E., & Byszewski, W. W. (1996). Microhollow Cathode Discharges. *Applied Physics Letters*,*68*(1), 13.

[2.15] Kogelschatz, U. (2007). Applications Of Microplasmas And Microreactor Technology. *Contributions to Plasma Physics*, *47*(1-2), 80-88.

[2.16] Mariotti, D., & Sankaran, R. M. (2010). Microplasmas For Nanomaterials Synthesis. *Journal of Physics D: Applied Physics*, *43*(32), 323001.

[2.17] Walsh, J. L., Iza, F., Janson, N. B., Law, V. J., & Kong, M. G. (2010). Three Distinct Modes In A Cold Atmospheric Pressure Plasma Jet. *Journal of Physics D: Applied Physics*, *43*(7), 075201.

[2.18] Wachtendorf, C., Herweg, C., Daeuber, M., Benedikt, J., & Keudell, A. v. (2009). Thin-film Growth From A Low Pressure Plasma Excited In A Supersonic Expanding Gas Jet. *Journal of Physics D: Applied Physics*, *42*(9), 095205.

CHAPTER 3: EXPERIMENTAL APPARATUS AND PROCEDURE

In this chapter, the experimental set up for the DC micro plasma jet performed in vacuum environment will be presented. SEM and orifice gas nozzle, which have played a crucial role in this research, will be introduced.

3.1 EXPERIMENTAL APPARATUS

3.1.1 SECONDARY ELECTRON MICROSCOPE (SEM)

SEM, or Secondary Electron Microscope, is an instrument that is used to observe objects in micro or nano scale. It is one type of electron microscope which produces images of the observed object by electron beam scanning [3.1]. The advantage is that it could observe an object whose size is smaller than a light wavelength with a high resolution better than 10 nanometer, which conventional optical microscopes cannot achieve [3.2]. The schematic drawing of SEM is shown in figure 3.1

To make an observation of the sample, the observing sample will be prepared and put on the sample stage of the Eucentric stage inside the SEM chamber [3.3]. The electron beam from the electron gun, accelerated by the bias voltage and focused by the electromagnetic lens (focusing lens and scanning lens), will be irradiated and the raster scanned on the sample surface. The electron beam diameter will be finally focused again by the objective lens. The electron interaction with sample atoms will produce various signals such as secondary electrons (SE), back-scattered electrons (BSE), characteristic X-rays, cathodoluminescence (CL), specimen current, and transmitted electrons. However, the most common mode of sample topography and morphology observation is secondary electron mode. The secondary electrons are emitted from the excited atoms on sample surface by the electron beam; therefore, the secondary electrons contain the information of the surface topography and morphology.

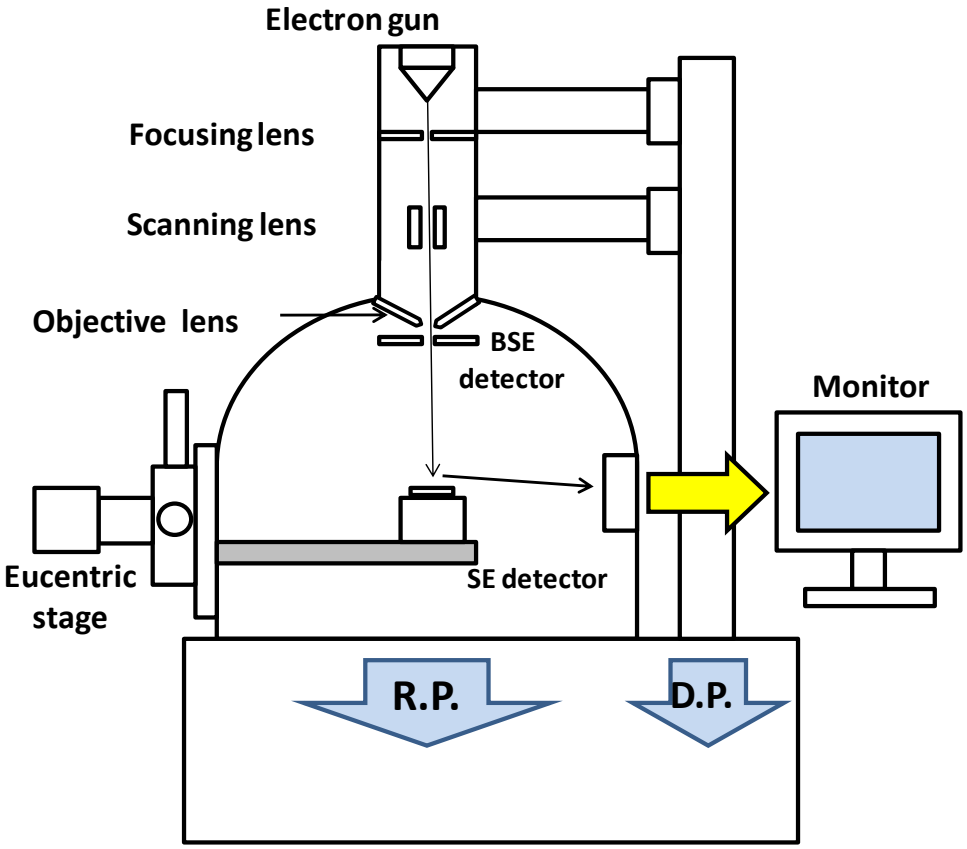

Figure 3.1 A schematic diagram of SEM.

By detecting the secondary electron signal by the secondary electron detector, the signal will be processed and finally [3.4-3.5] displayed on the SEM monitor. It should be emphasized that to operate SEM observation, the SEM chamber should be in a high vacuum environment (around 1.5×10^{-3}Pa) to avoid the interference from other gas and the damage of the electron gun. Therefore, rotary pump (R.P) and oil diffusion pump (D.P.) are necessary to maintain the vacuum environment in SEM during operation. Figure 3.2 presents the Hitachi SEM S-3000N, which is used for micro plasma jet generation in this research.

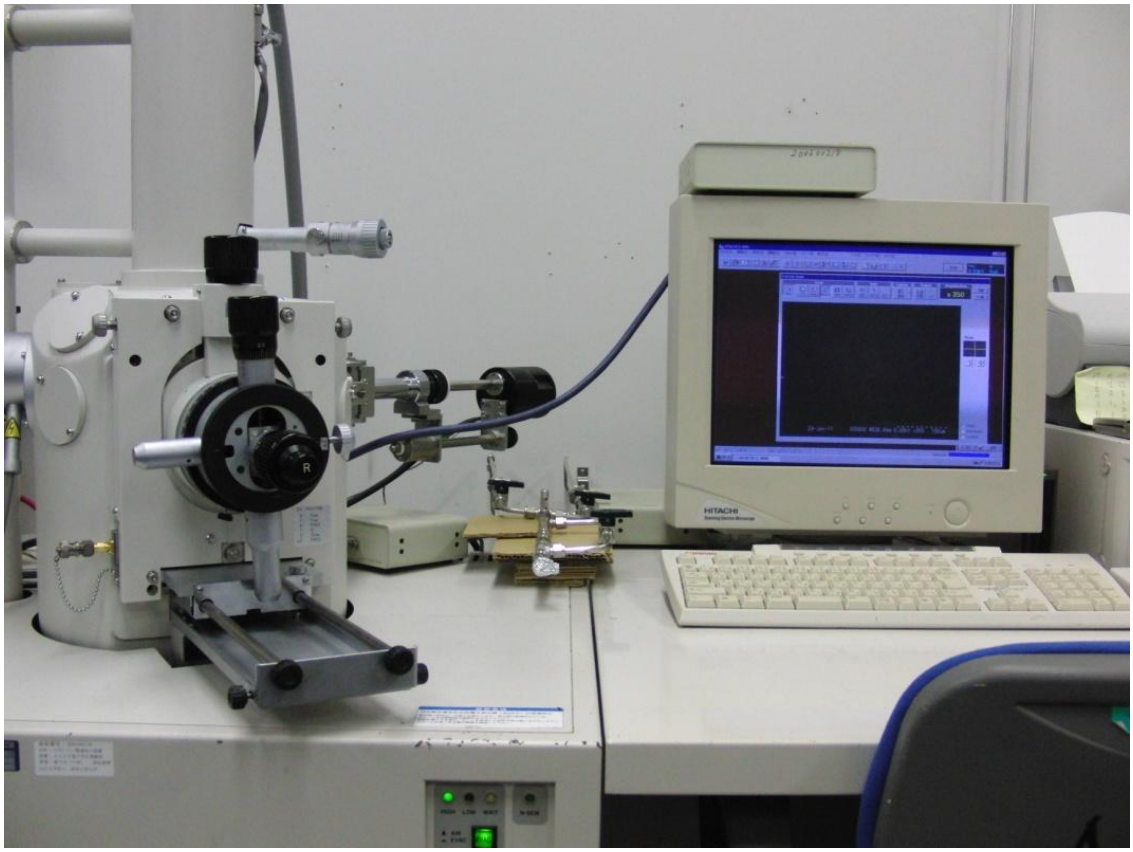

Figure 3.2 Hitachi SEM S-3000N.

3.1.2 ORIFICE GAS NOZZLE

The usage of orifice gas nozzle (OGN), consisting of a small hole on a thin wall, is a key issue for injection of localized high pressure micro gas jet into a vacuum environment. Otherwise, by using a micro capillary type gas nozzle, the pressure of injected gas becomes too small to operate gas discharge due to the poor conductance of long capillary tube.

Figure 3.3 illustrates the fabrication process of ordinary orifice handmade gas nozzle made by our research group. The orifice gas nozzle was made from an 8 cm length stainless steel tube having inner and outer diameters of 1.45 and 1.81 mm, respectively. To close the tube at the end of one side, the stainless steel tube, consisting of the tungsten (W) wire having a diameter of 30 µm (the size of the wire is dependent on the desired OGN hole size), is molded by the swaging machine. After the tube is shaped similarly to the mold shape, a rasp is used to grind the closed-end tube tip until the W wire can be pulled out; this step implies that a small hole may then be achieved. The small hole from the closed-end tube surface can be confirmed by an optical microscope and SEM machine. The successful orifice gas nozzle having a 40 µm hole diameter made by this method is shown in figure 3.4.

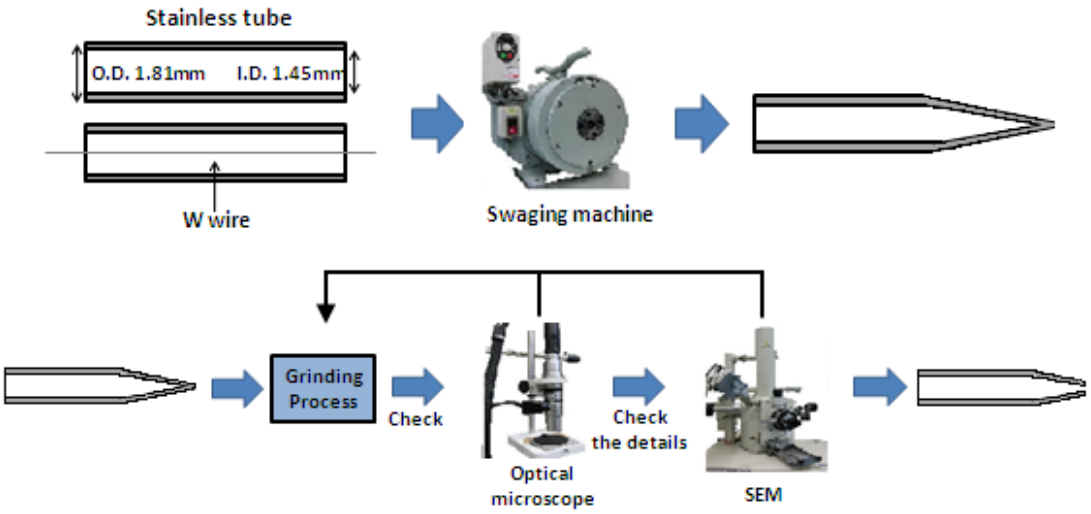

Figure 3.3 Fabrication flow chart of the ordinary orifice gas nozzle made by our research group.

Figure 3.4 A stainless steel tube and the surface of orifice gas nozzle

The orifice conductance has the ability to convey the gas flow. It could be simply estimated by the ratio of supplying gas flow rate and the pressure inside the orifice gas nozzle [3.6]. The small hole on the orifice gas nozzle surface, compared to the main capillary tube diameter on a thin wall surface, will cause the small orifice conductance. For example, at the Argon gas flow rate of 2.5 sccm, the pressure inside the orifice gas nozzle could be high as 20 kPa; therefore, this OGN has the conductance of 0.125sccm/kPa. Due to the small orifice conductance, the pressures inside of OGN and at the exit of orifice would be close to the applied pressure, which enables localizing high gas jet inside the vacuum environment as noticed by the SEM gas jet profile (gas profile will be discuss later). However, due to the difficulty in the fabrication process and poor reproducibility, the ordinary handmade orifice gas nozzle is replaced by the commercial one fabricated by Lenox Laser [3.7]. The Lenox orifice gas nozzle is depicted in figure 3.5.

http://www.lenoxlaser.com

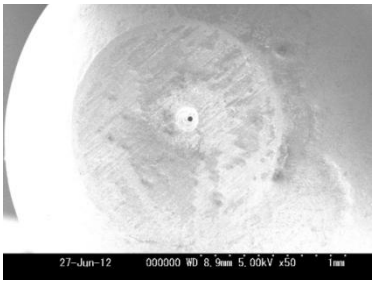

Figure 3.5 Lenox orifice gas nozzle and its SEM image of 30 μm hole at the nozzle surface.

3.2 EXPERIMENTAL SET UP AND PROCEDURE

The experiments in this research were conducted inside an SEM (Hitachi S-3000N) chamber; the schematic drawing of experimental set up is illustrated in figure 3.6. The anode of an OGN was supported by a 3-D micro-manipulator in the chamber. At the cathode side, a cut of mirror polished with Si wafer of low resistivity was placed on another 3-D micro-manipulator vertically and counter to the OGN. The gap distance between the electrodes was adjusted, ranging to about 300 μm by monitoring the scale in the SEM image.

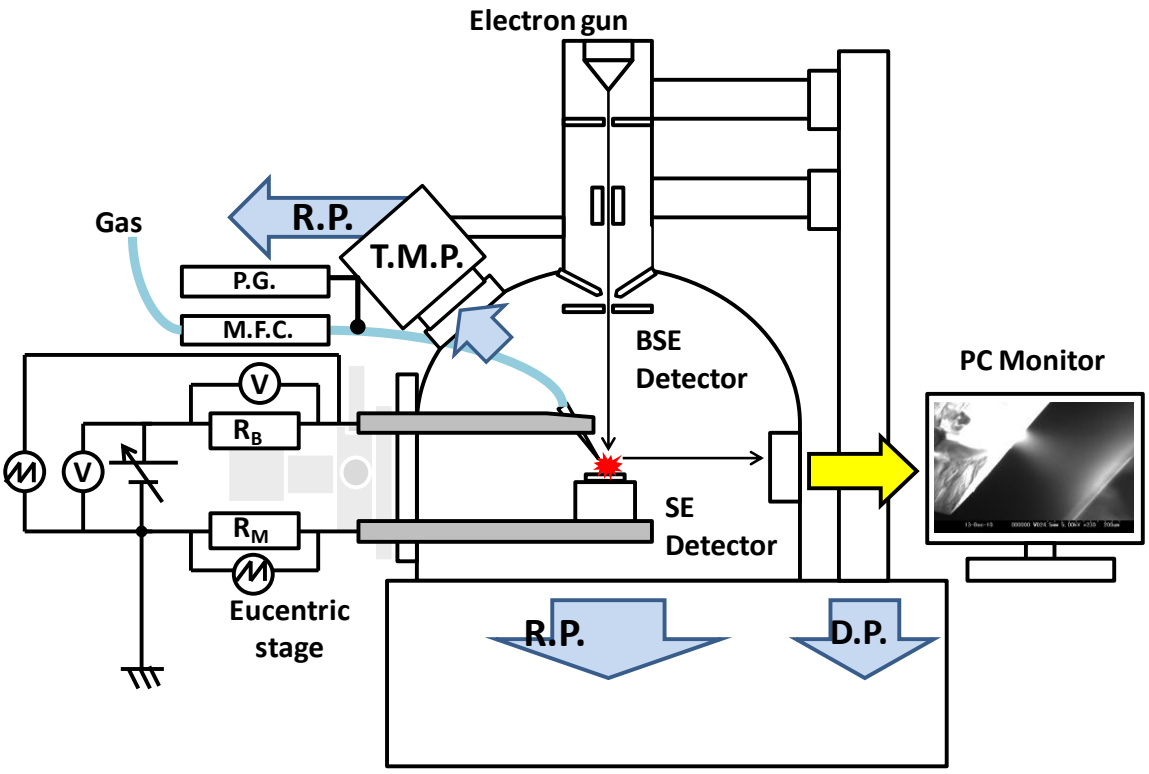

Figure 3.6 A schematic diagram of the micro gas jet set up in SEM observation chamber.

Argon gas was supplied to the OGN through a mass flow controller (MFC). The presented OGN (Lenox Laser) was a standard 1/8" (D) SS-316 tubing closed at one end, with a laser-drilled hole (d) 30 μm in diameter; its schematic drawing is

shown in figure 3.7. The Argon pressure applied to the orifice, monitored by a pressure gauge, was proportional to the gas flow rate of MFC. The conductance of the OGN as the ratio of gas flow rate to the applied pressure was about 0.075 sccm/kPa. A turbo molecular pump (PFEIFFER VACUUM, TMU071YP) was installed on a service port on the side wall of the chamber, in addition to the original vacuum system. With injection of micro gas jet up to 20 sccm flow rate, which was the maximum in the present experiments, the chamber pressure was kept below 1 Pa and the SEM worked in the normal operating conditions.

Figure 3.7 A schematic drawing for Lenox orifice gas nozzle.

A positive voltage was applied to the OGN from a DC power source of 1 kV at maximum, through a 10 MΩ ballast resistor (R_B). The discharge voltage and current were monitored using a set of digital multi-meters (DMM). One was used for measuring the source voltage, and the other was used for measuring the voltage drop across the ballast resister R_B which reflected the discharge current (I_d). The applied voltage to the OGN (discharge voltage) was obtained by the difference between the measured voltages. The discharge voltage and current sometimes pulsated due to oscillation in the circuit, while the source voltage was kept constant. The monitored voltage and current, by the multi-meters at a small sampling rate of 2 samples/s, represented time averaged values when the discharge was automatically pulsating at frequencies around a several kHz. For measuring the real pulsating current, the counter electrode of Si substrate was grounded by a 50 Ω through a terminator (R_M), and inserted

into a BNC cable line. And for measuring the real discharge voltage of OGN, a high voltage probe was connected to the OGN. The current and voltage waveforms for the pulsating mode were stored in a digital oscilloscope (IWATSU-LeCroy, LT364).

3.3 MICRO PLASMA JET GENERATION IN SEM CHAMBER

3.3.1 ELECTRON BEAM ENHANCED MICRO PLASMA JET GENERATION IN SEM CHAMBER

In this research, the experiments were performed in a SEM chamber. One of the advantages of generating micro plasma in a SEM chamber is that the breakdown voltage (V_{BR}) of plasma can be reduced by electron beam. In figure 3.8, breakdown voltage at various gas flow rates, comparing between when the electron beam is on or off (at the gap distance of 50 μm and orifice hole diameter of 80 μm), is presented. Breakdown voltage can be determined by observing the SEM monitor after Argon gas is fed through the orifice and voltage was supplied for plasma generation. The SEM monitor screen becomes white, due to abundant electrons from the gas discharge when plasma exists in the SEM chamber. The SEM monitor and oscilloscope were both observed during plasma generation to confirm whether the plasma was stable or not in this research. When the electron beam of SEM was operated, V_{BR} became lower than that without the beam due to ignition of discharge by electron beam [3.8-3.9].

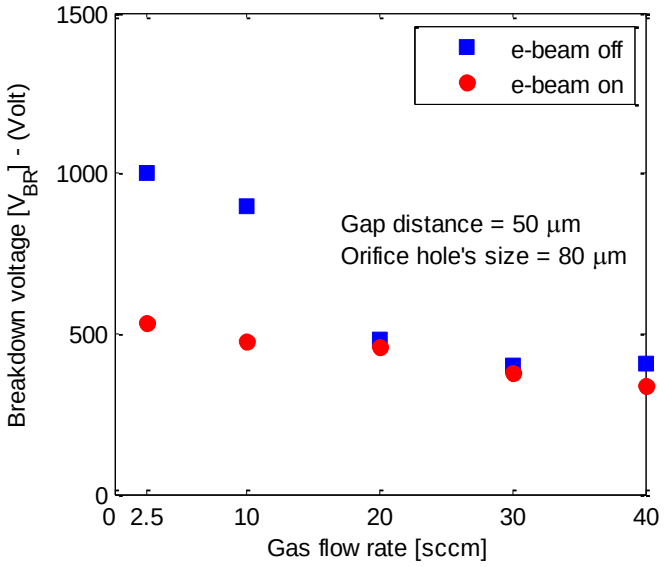

Figure 3.8 Breakdown voltage (V_{BR}) at various gas flow rates, comparing between when the electron beam is on or off at the gap distance of 50 μm and orifice diameter of 80 μm.

The results show that almost every experiment, in the case of generating plasma without electron beam, has higher V_{BR} than that with electron beam. This is due to the extremely small chance of finding a primary electron in a small micro electrode gap where there is no electron beam [3.10]. It is difficult for primary electrons from background radiation, for example Cosmic ray and radioactive minerals, to pass through the small gap to ignite plasma. Plasma generation has to wait until the primary electron happens to travel into the small gap between the orifice gas nozzle and substrate. Therefore, V_{BR} without electron beam is determined by the supplied voltage at the time that primary electron arrives between micro gap. From figure 3.8, it could be noticed that the V_{BR} is decreased when the GFR and OGP increases. On the contrary, at the constant OGP and at various electrode gap distances, the V_{BR} increases when the gap distance is increased. These two results could be implied that the V_{BR} is dependent on the gas pressure gradient at each electrode gap distance. Therefore, the Paschen's equation in this research should be modified into $V_{BR} = f(\nabla p(d).d)$.

3.3.2 MICRO GAS JET PROFILE BY SEM

One more interesting advantage of generation of micro plasma jet inside SEM, is that the gas profile of injecting gas through the orifice could be observed.

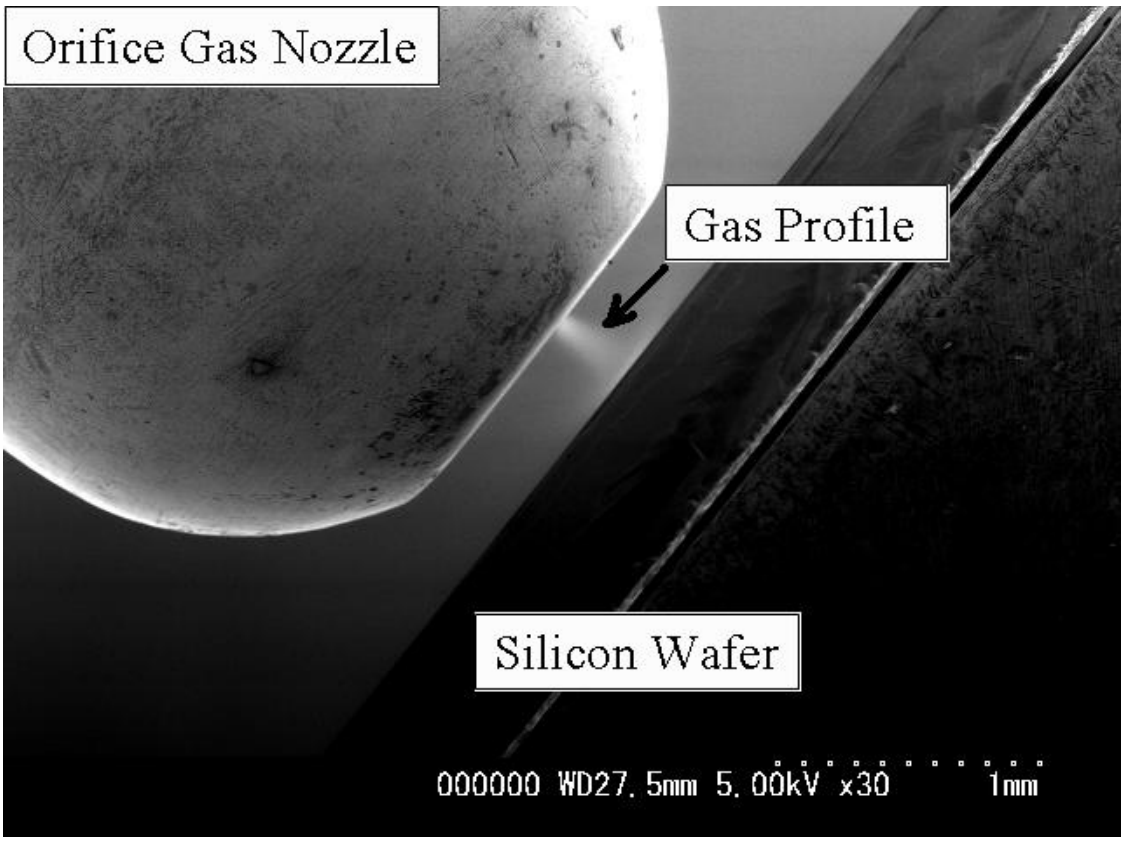

Figure 3.9 A SEM image of the OGN anode and Si cathode with Argon micro gas jet.

Figure 3.9 shows a typical SEM image of the gas jet between the OGN and Silicon wafer cathode at 15 sccm flow rate, 210 kPa orifice gas pressure (OGP), and 300 μm gap distance. Because the conductance of the straight part of OGN (3 mm inner diameter, D) was sufficiently larger than that of the small end orifice (30 μm, d), as depicted in figure 3.7, the pressures inside of OGN and at the exit of orifice would be close to the applied pressure. This factor results in the possibly localized gas jet inside the vacuum environment.

Gas profile is the characteristic of the injected gas from the exit of orifice gas nozzle, into a vacuum environment. The gas profile could be observed by SEM observation, which is one advantage of generating plasma inside SEM. The gas molecules were ionized by the scanning electron beam, and the produced electrons were detected in the same way as the detection of secondary emission from solid surfaces. The brightness of the image depends on the total accumulated number density of gas molecules, along with the beam line passing through the gas jet. Due to the gas profile, the gas flow condition could be observed. It could be noticed from the gas profile that there are two flow conditions: viscous flow and turbulent flow. These two gas flow modes cause a large gradient of gas pressure, and they could be distinguished by the brightness of gas profile observed by SEM. The viscous flow could be observed at the exit of OGN (brighter colour column), while turbulent flow exists after the viscous flow at about a few 10 μm far from the exit of OGN. The turbulent gas flow profile has the dimmer brightness due to the fast diffusion rate. This characteristic of flowing injected gas is useful for estimating the gas jet diameter and plasma size.

3.4 SUMMARY

The experimental set up for the DC micro plasma jet performed in vacuum environment was presented. Due to a small conductance orifice, the local gas jet could be achieved, and the micro plasma jet could be successfully generated inside the SEM chamber. The advantage of plasma operation inside SEM is that the electron beam from SEM serves the primary electrons, which is hardly found in the very small electrode gap for plasma ignition. Moreover, the gas profile could be observed by SEM observation and it is useful for estimating plasma size.

3.5 REFERENCES

[3.1] Oatley, C. W. (1972). *The Scanning electron microscope*. London: Cambridge University Press.

[3.2] Wells, O. C. (1974). *Scanning electron microscopy*. New York: McGraw-Hill.

[3.3] Hayat, M. A. (1978). *Introduction to biological scanning electron microscopy*. Baltimore: University Park Press.

[3.4] Hearle, J. W., Sparrow, J. T., & Cross, P. M. (1972). *The use of the scanning electron microscope,* ([1st ed.). Oxford: Pergamon Press.

[3.5] Lyman, C. E. (1990). *Scanning electron microscopy, X-ray microanalysis, and analytical electron microscopy: a laboratory workbook*. New York: Plenum Press.

[3.6] Chapman, B. N. (1980). *Glow discharge processes: sputtering and plasma etching*. New York: Wiley.

[3.7] Flow control orifices: Lenox Laser. (2003 Reader's Choice Awards). (2003, March 1). *Laboratory Equipment*.

[3.8] Mizobuchi, Y., Fukunaga, K., Tojo, N., Tatsugawa, T., Sakai, T. and Hatta, A. (2009). "Discharge characteristics for micro-gas jet in vacuum", paper presented at *The 27th Symposium on Plasma Processing*, Yokohama, pp.113-115.

[3.9] Matra, K., Mitzobuchi, Y., Furuta, H. and Hatta, A. (2011). "Local sputtering by micro plasma jet in SEM", paper presented at *11th international symposium on Sputtering & Plasma Process*, Kyoto, pp. 46-49.

[3.10] Zou, Q., Kanakusa, H., Yoshimura, H., & Hatta, A. (2006). Pulsed Microplasma Using Carbon Nanotubes For Cathode.*Japanese Journal of Applied Physics*,*45*(No. 10B), 8225-8227.

CHAPTER 4: CURRENT-VOLTAGE CHARACTERISTICS OF DC MICRO PLASMA JET INJECTED INTO A VACUUM ENVIRONMENT

This chapter aims to study the electrical characteristics of DC gas discharges operated in a micro gas jet injected in the SEM chamber. The current and voltage characteristics were studied with a variety of supplied pressure, electrode gap distance and source voltage. The real time plots of self-pulsing voltage and current was investigated using a discharge model [4.1].

4.1 EXPERIMENTAL PROCEDURE

Almost all the experimental set up for the study of current-voltage characteristics of the dc micro plasma jet injected into a vacuum environment in this chapter have already been explained in section 3.2, chapter 3. The parameters which differed were as follows: the gap distance between the electrodes was adjusted to 100, 200, and 300 μm. The orifice gas nozzle used in this section, was a standard 1/8" SS-316 tubing closed at one end with a laser-drilled hole 30 μm in diameter (Lenox Laser). The conductance of the OGN was about 0.075 sccm/kPa.

4.2 EXPERIMENTAL RESULTS AND DISCUSSION

4.2.1 VOLTAGE-CURRENT CHARACTERISTICS OF THE DISCHARGE IN MICRO-GAS JET IN A VACUUM

Figure 4.1 shows the plots of voltage and current monitored by the multi-meters with the variation of gap length and the applied pressure (OGP). The data was obtained by first supplying Argon gas to OGN, which was already set G_d between the counter electrodes in the SEM chamber, then gradually increasing supplied voltage. Plasma was expected to be stable if the discharge waveforms, which can be noticed on the oscilloscope monitor, performed in linear waveform. The obtained V-I curves almost

follow the conventional characteristics of glow discharge, i.e., constant voltage with variation of current. By increasing the source voltage while the discharge voltage remained almost constant, the discharge current, limited by the ballast resistance, gradually increased.

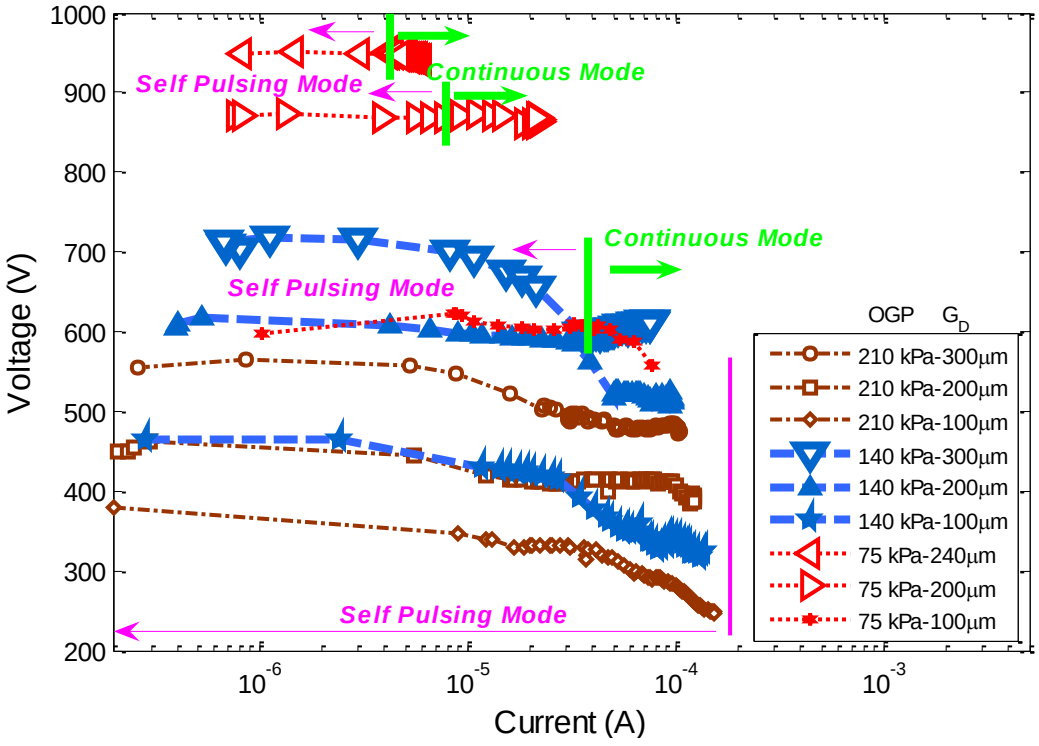

Figure 4.1 Plots of time averaged voltage and current for discharge in a micro gas jet in a vacuum monitored by the multi-meters.

Figure 4.2 shows typical waveforms of voltage and current monitored by the oscilloscope at the experimental condition of 300 μm gap and 140 kPa pressure. There were two different modes of discharge observed, self-pulsating mode and continuous mode [4.2-4.7]. The discharge at 800 V (source voltage, V_S) was automatically pulsating even if the source voltage was kept constant [4.8]. The discharge at 1,000 V_S was stable and continuous at the constant voltage and the constant current. It

has been confirmed that the continuous discharge mode is suitable for local plasma processing like as micro sputter etching due to their stability [4.9].

V-I characteristics of Argon micro gas jet discharge in figure 4.1 were quite different from the conventional glow discharge V-I characteristic graph, because the gas pressure between electrodes in this research was not constant. When Argon gas is fed through OGN, gas will disperse and will be evacuated very rapidly. Therefore, the pressure rapidly decreased according to the distance from OGN. This situation causes non uniform gas profile [4.10].

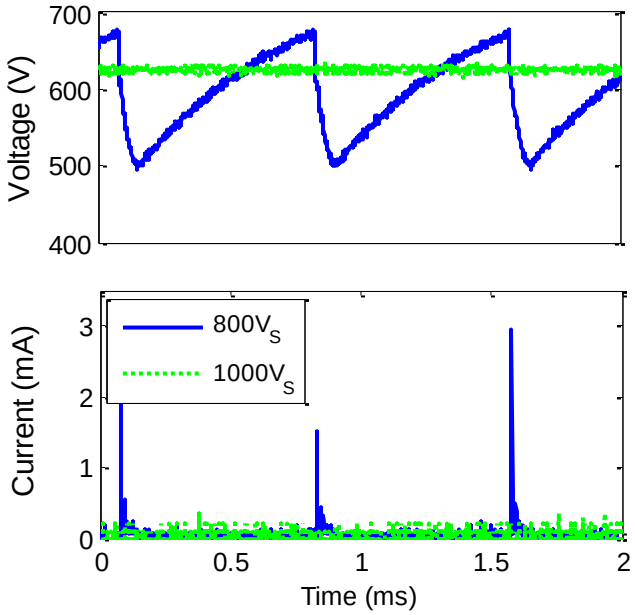

Figure 4.2 Waveforms of voltage and current monitored by the oscilloscope at 300 μm gap, 140 kPa pressure, and 800 V and 1,000 V source voltages (V_S).

Actually, figure 4.1 includes both the plots for the stable continuous discharge mode which represent real voltage and current, and also the hypothetical plots of time average for the self-pulsing discharge mode. The thick lines plotted in figure 4.1 show the results in which the discharge mode transited from the self-pulsating mode to

the continuous mode when the monitored current exceeded critical current values as indicated. The minimum current to sustain continuous gas discharge (I_{min}) depended on pressure, electrode gap distance, and other factors. All the plots on the thin lines show the apparent values on digital multimeter for self-pulsating mode. The continuous mode was observed at the lower pressure (75 kPa) when the current exceeded 20 and 5.68 μA at the gap distance of 200 and 240 μm, respectively. At the medium pressure (140 kPa) the continuous mode appeared at the gap length 300 μm when the current exceeded 40 μA. At the higher pressures, 140 and 210 kPa, and at the shorter gap distance, the discharge was always pulsating even if the current was increased until the maximum source voltage.

As shown in figure 4.2, the current waveform at 800 V_S consists of sharp pulses with peak current ranging from 2-3 mA repeating with intervals about 0.75 ms. At 1,000 V_S, the discharge current was stable and continuous at about 70 μA as indicated in figure 4.1. The peak current in the self-pulsing mode was 30 to 40 times larger than that for the continuous mode. In the self-pulsing mode, the voltage dropped abruptly during the short pulses of discharge current and gradually increased during the intervals resulting in saw tooth wave. The pulsating frequency, mostly determined by the interval length, ranged in 0.5-5 kHz depending on the pressure, gap length, and also the source voltage.

4.2.2 SELF-PULSING DISCHARGE OSCILLATED IN THE CIRCUIT

Figure 4.3 shows typical waveforms of voltage and current during pulsating mode in the enlarged time scale for the experimental condition at 210 kPa pressure, 200 μm gap length and 800 V source voltage. Figure 4.4 shows the real plots of instantaneous current and voltage for the self-pulsing discharge at 210 kPa pressure, 200 μm gap length with variation of source voltage including the data shown in figure 4.3.

The self-pulsing mode is characterized by two threshold voltages. One is sustained voltage or recovery voltage as the minimum voltage to sustain plasma (V_{RE}) and the other is breakdown voltage as the maximum (V_{BR}) [4.11]. For the self-pulsating mode, the discharge voltage oscillated between these two voltages as indicated in figure 4.3 and 4.4. The discharge current appeared in the period of voltage drop from V_{BR} to V_{RE}.

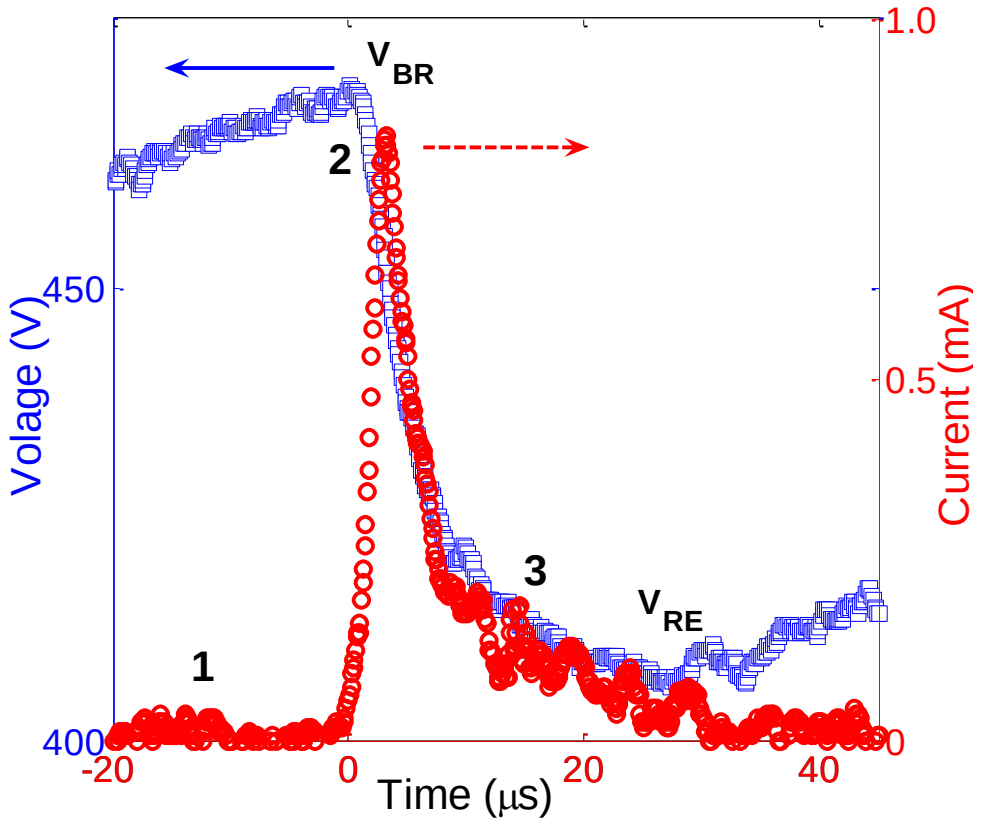

Figure 4.3 Typical waveforms of voltage and current during self-pulsing mode in the enlarged time scale at 210 kPa pressure, 200 μm gap, and 800 V_S.

The self-pulsing of the discharge can be divided into 3 phases as depicted in figure 4.3. The 1st phase is increasing voltage during the intervals of discharge, the 2nd phase is increasing of discharge current with abrupt decrease of voltage, and the 3rd

phase is decreasing of discharge current with also abrupt decrease of voltage to terminate until the voltage decreased to V_{RE} [4.12-4.13].

In the 2nd phase, in the present result, the discharge current abruptly increased to 0.83 mA within the rising time of 4.8 μs and the voltage dropped from 472 V to 453 V. In the 3rd phase, the discharge current decreased from the peak to around 50 μA within 16 μs together with decreasing of voltage from 453 V to V_{RE} (405V). After diminishing the discharge, the voltage increases to V_{BR} (472 V) again. This process was periodically repeated resulting in the self-pulsating discharge.

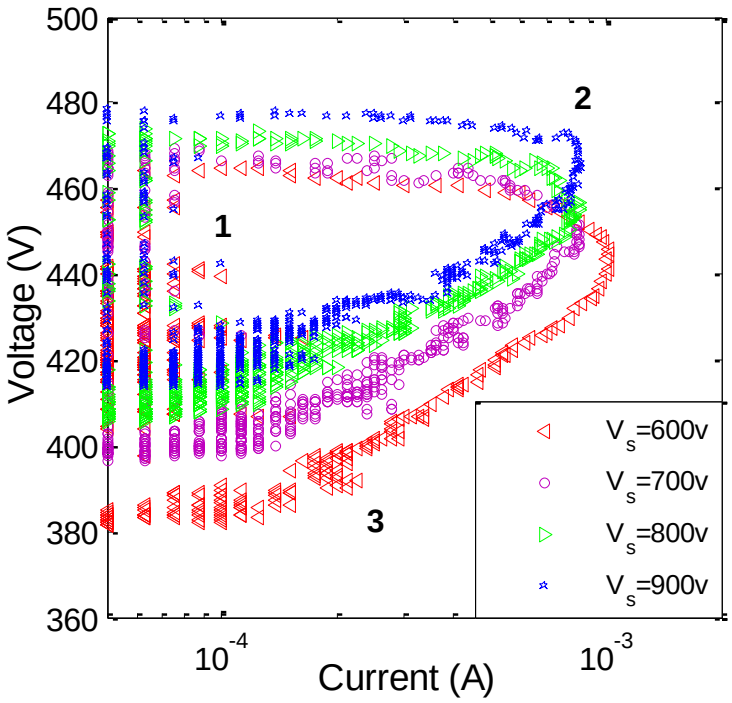

Figure 4.4 Real plots of instantaneous voltage and current for the self-pulsing mode at 210 kPa pressure, 200 μm gap, and variation of source voltage (V_S).

In figure 4.4, it should be noticed that, even at the same condition for gas discharge, the observed breakdown voltage V_{BR} and the minimum sustain voltage V_{RE} varied with variation of the source voltage. It is necessary to explain the reason why the voltage source affected the discharge characteristics.

For the minimum voltage, V_{RE}, the observed value was not the minimum sustain voltage for the discharge but just the turning voltage from decreasing phase to the recovery phase. By carefully looking at the transition from the 3rd phase to the next 1st phase, i.e., at the termination of the discharge, the voltage has started to recover before the current disappears completely. Because the current was continuously supplied through the ballast resistance also during the discharge, the minimum voltage V_{RE} appeared at the time when the discharge current decreased to the supplying current. When the discharge current was decreased to the supplying current, the actual voltage turned to increase before termination of discharge. When the source voltage was increased, due to increase of the supplying current through the ballast resistance, the decreasing of voltage was terminated faster and started to recover at the higher voltage.

For the breakdown voltage, it should be necessary to consider the pre-ionization before the distinctively observed current pulse. When the voltage approached the real breakdown voltage, ionization started to build up the plasma column and finally to ignite the main discharge. It will take a few μs for building up the plasma column. Due to the delay of building up the main discharge after the voltage became the breakdown voltage, the observed V_{BR} was exceeded the real breakdown voltage. When the source voltage was increased, the working voltage was increased more rapidly during the delay time resulting in observation of higher maximum voltage at the ignition of main discharge.

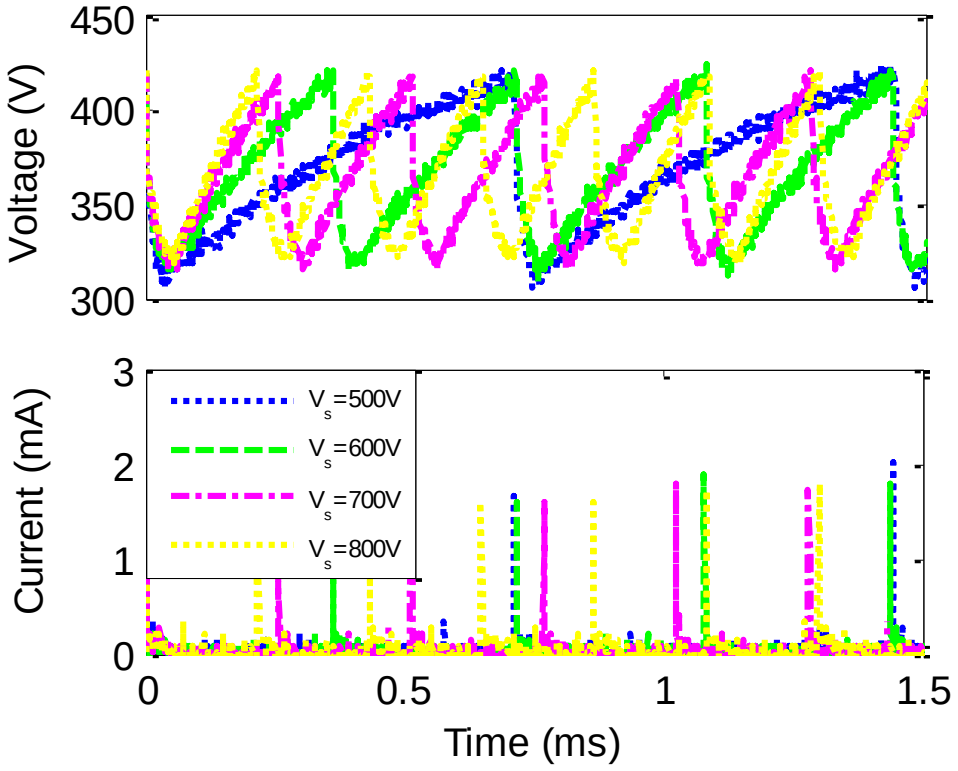

Figure 4.5 Voltage and current waveforms with variation of the applied voltage at 210 kPa pressure and 100 μm gap.

Figure 4.5 shows the voltage and current waveforms with variation of source voltage (V_S) at the same discharge condition of self-pulsing mode, 210 kPa pressure and 100 μm gap. The pulsating frequency increased with increasing the source voltage. Figure 4.6 shows a model for the electrical circuit of discharge including the stray capacitor.

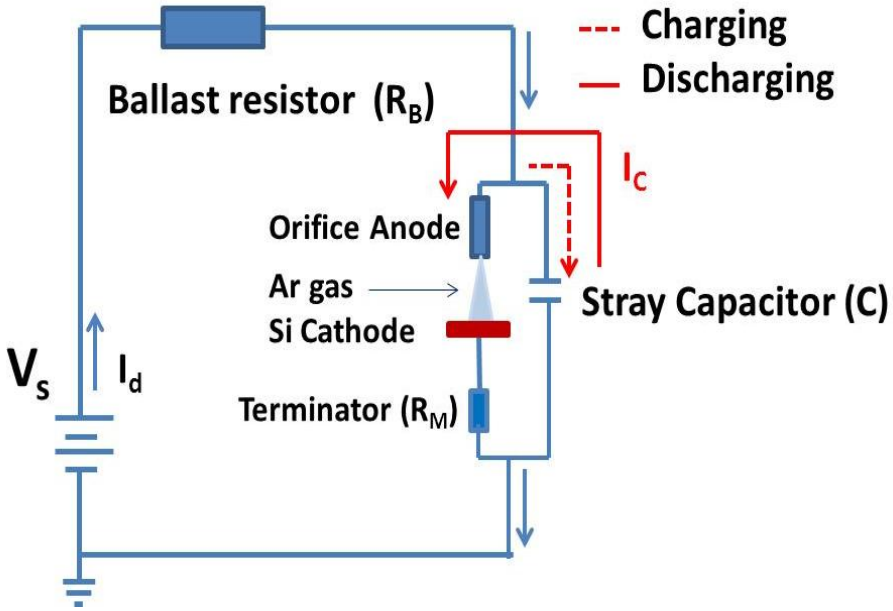

Figure 4.6 Model for the voltage oscillation due to charging and discharging of the stray capacitance through the ballast resistance.

During the interval of discharge, the stray capacitor was charged through the large ballast resistor until the gas breakdown voltage. When the voltage exceeded the breakdown voltage, the gas discharge started to flow the electrical current with discharging the stray capacitor. When the current supplied from the ballast resistor was sufficient to sustain the continuous discharge ($I_d \geq Imin$), the continuous mode of discharge started. If the current supply from the power source through the ballast resistor was insufficient for sustaining the continuous discharge ($I_d < I_{min}$), the discharge was automatically terminated and the stray capacitor was charged again until the breakdown voltage. Therefore, I_{min}, the minimum current to sustain continuous discharge, was the threshold between the self-pulsing mode and continuous mode.

When the source voltage (V_S) was increased, the supplied current through the ballast resistor increased resulting in rapid recovery of voltage for the next discharge of ignition and higher frequency of pulsating. When the ballast resistor was decreased, the supplied current increased with resulting in higher frequency [4.14]. The trends of charging the stray capacitor simply follow the RC oscillation circuit model. In the present experiments, the stray capacitor was about 65 pF. It has been confirmed that the most of stray capacitor existed in the coaxial high voltage cable between the ballast resistor and the electrode.

The self-pulsing discharge also could be controlled by varying ballast resistor and stray capacitor [4.5, 4.14-4.15]. Due to the extreme peak power together with controllable pulse frequency, the self-pulsing mode is also applicable for micro plasma processing [4.14-4.16].

4.3 SUMMARY

Characteristic of current and voltage of discharge operated in micro gas jet injected into vacuum environment was investigated using the orifice of 30 μm diameter for anode and the Si substrate for cathode equipped in the SEM. The discharge showed self-pulsing mode and continuous mode. The continuous discharge occurred at lower pressure gas jet with longer gap distance at larger current. The self-pulsing of voltage and current was investigated using a model of discharge circuit including stray capacitor. The self-pulsing and continuous discharge mode can be distinguished by I_{min}, which is the minimum current to sustain continuous discharge.

4.4 REFERENCES

[4.1] MATRA, K., Furuta, H., & Hatta, A. (2013). Current-Voltage Characteristics of DC Discharge in Micro Gas Jet Injected into Vacuum Environment. *Journal of Physics: Conference Series*, *441*(1), 012021.

[4.2] Staack, D., Farouk, B., Gutsol, A., & Fridman, A. (2008). DC Normal Glow Discharges In Atmospheric Pressure Atomic And Molecular Gases. *Plasma Sources Science and Technology*, *17*(2), 025013.

[4.3] Shirai, N., Nakazawa, M., Ibuka, S., & Ishii, S. (2009). Atmospheric DC Glow Microplasmas Using Miniature Gas Flow And Electrolyte Cathode. *Japanese Journal of Applied Physics*, *48*(3), 036002.

[4.4] Arkhipenko, V. I., Kirillov, A. A., Safronau, Y. A., and Simonchik, L. V. (2012) DC atmospheric pressure glow microdischarges in the current range from microamps up to amperes. *The European Physical Journal,* 60(3), 455-463.

[4.5] Yokoyama, T., Hamada, S., Ibuka, S., Yasuoka, K., & Ishii, S. (2005). Atmospheric Dc Discharges With Miniature Gas Flow As Microplasma Generation Method. *Journal of Physics D: Applied Physics*, *38*(11), 1684-1689.

[4.6] Aubert, X., Bauville, G., Guillon, J., Lacour, B., Puech, V., & Rousseau, A. (2007). Analysis Of The Self-pulsing Operating Mode Of A Microdischarge.*Plasma Sources Science and Technology*,*16*(1), 23-32.

[4.7] Du, B., Mohr, S., Luggenhölscher, D., & Czarnetzki, U. (2011). An atmospheric pressure self-pulsing micro thin-cathode discharge. *Journal of Physics D: Applied Physics*, *44*(12), 125204.

[4.8] He, S., Ouyang, J., He, F., & Jia, H. (2012). Self-pulsing operating mode of hollow cathode discharge in noble gas.*Physics of Plasmas*, *19*(2), 023504.

[4.9] Matra, K., Mitzobuchi, Y., Furuta, H. and Hatta, A. (2013). Local sputter etching by micro plasma jet in SEM. *Vacuum, 87,* 132–135.

[4.10] Bardos, L., & Barankova, H. (2008). Plasma Processes At Atmospheric And Low Pressures. *Vacuum*, *83*(3), 522-527.

[4.11] Ovidiu. S., and STOICAN. J. (2009) Effect of an external electrode on the characteristics of a low frequency discharge. *Journal of Plasma and Fusion Research SERIE,* 8, 804-808.

[4.12] Lazzaroni, C., & Chabert, P. (2011). Discharge Resistance And Power Dissipation In The Self-pulsing Regime Of Micro-hollow Cathode Discharges. *Plasma Sources Science and Technology*, *20*(5), 055004.

[4.13] Rousseau, A., & Aubert, X. (2006). Self-pulsing Microplasma At Medium Pressure Range In Argon. *Journal of Physics D: Applied Physics*, *39*(8), 1619-1622.

[4.14] Wu, S., Lu, X., Xiong, Z., & Pan, Y. (2010). A Touchable Pulsed Air Plasma Plume Driven By DC Power Supply. *IEEE Transactions on Plasma Science*, *38*(12), 3404 - 3408.

[4.15] Lu, X., Wu, S., Chu, Paul. K., Liu, D., and Pan, Y. (2011) An atmospheric-pressure plasma brush driven by sub-microsecond voltage pulses. *Plasma Sources Science and Technology. 20(6),* 065009.

[4.16] Staack, D., Farouk, B., Gutsol, A., & Fridman, A. (2005). Characterization Of A Dc Atmospheric Pressure Normal Glow Discharge. Plasma Sources Science and Technology, 14(4), 700-711.

CHAPTER 5: LOCAL SPUTTER ETCHING BY MICRO PLASMA JET IN SEM

Since the characteristics of DC micro plasma jets operated inside SEM have already been studied in chapter 4, this chapter will apply this system to micro sputter etching. The local micro sputter etching in SEM is expected to be used for fabrication of micro-electromechanical system devices (MEMS) and local restoration of micro-electronics devices such as large scaled integrated circuits (LSIs) with low contamination. In this chapter, local micro sputter etching by DC Argon (Ar) plasma using a small orifice gas nozzle in an SEM chamber will be presented. There will also be a discussion of the important role gap distance (G_d), gas flow rate (GFR), discharge time (T_d) and discharge current (I_d), play in the characteristics of local sputtering [5.1].

5.1 EXPERIMENTAL PROCEDURE

Most of the experimental set up for the current-voltage characteristics of dc micro plasma jets injected into a vacuum environment discussed in this chapter have already been explained in section 3.2, chapter 3. In this section, the ordinary orifice gas nozzle (OGN) fabricated by our research group was used. The OGN was made from a stainless steel tube with a hole size of 40 μm and inner and outer diameters of 1.63 and 1.81 mm respectively, as depicted in figure 5.1. Si substrate, which is the OGN counter electrode, was placed at G_d of 50, 100, 150 and 200 μm.

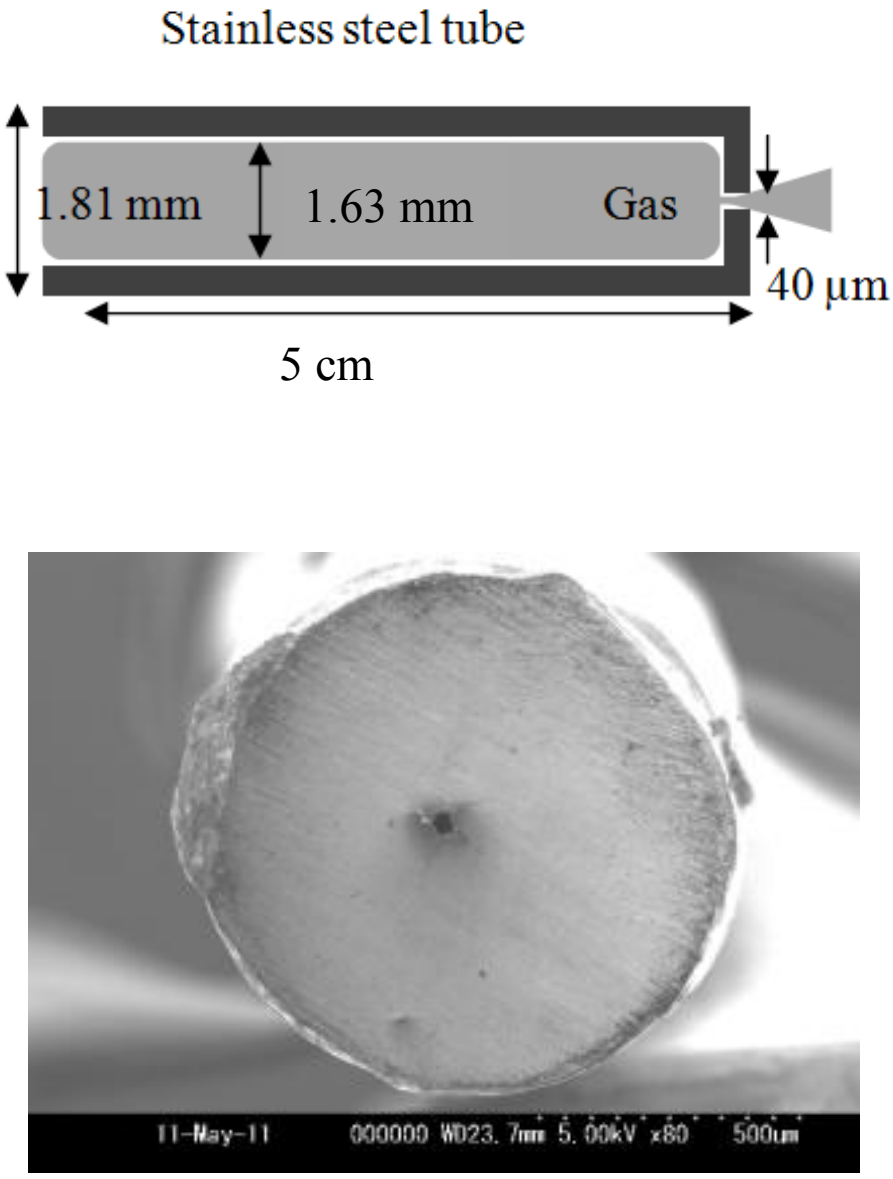

Figure 5.1 Schematic drawing of orifice gas nozzle used for micro sputter etching and the SEM image of its surface.

5.2 EXPERIMENTAL RESULTS AND DISCUSSION

5.2.1 CHARACTERISTICS OF MICRO PLASMA JET IN SEM

Since the orifice gas nozzle differs from that of the previous chapter, the voltage-current (V-I) characteristics of the micro plasma jet generated by the new OGN is here discussed. Figure 5.2 presents the V-I characteristics of Argon micro gas jet discharge at the various GFR and G_d. The data were obtained by supplying Argon gas to OGN which was already set G_d between the counter electrodes in SEM chamber, then increasing supplied voltage gradually. In order to determine plasma stability, if the discharge waveforms, which can be noticed on the oscilloscope monitor, were performed in linear waveform, plasma was expected to be stable. It was noticed that the V-I characteristic graphs in the interested discharge current range (10^{-6} A) display two different styles of slope. Firstly, a slight negative slope could be found in the case using short G_d and high GFR. Secondly,

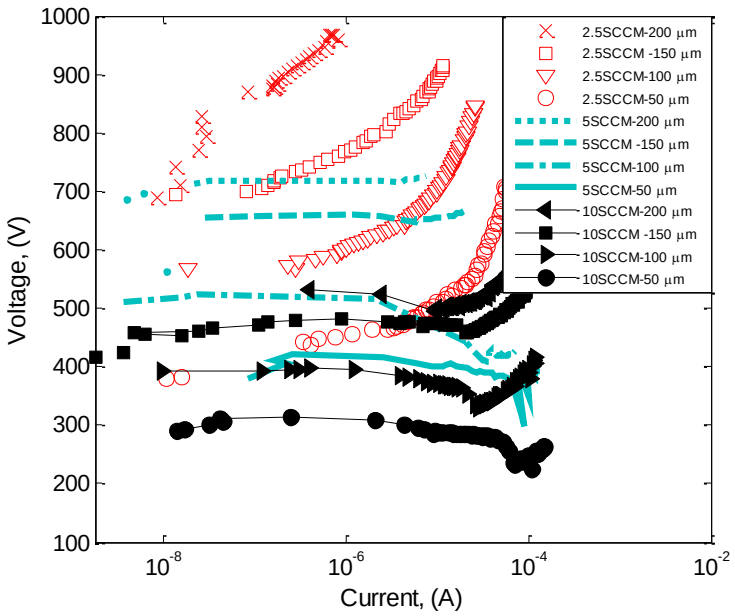

Figure 5.2 Voltage-current (V-I) characteristics of Argon micro discharge at various gap distance and gas flow rate.

a positive slope could be seen in the case using long G_d and low GFR. Stable gas discharge was found in long G_d and low GFR condition. The slightly negative slope of the V-I characteristic graphs in the first case are phenomenon in normal glow discharge region. When the discharge current is increased, the discharge area diameter is also expanded with constant current density until the discharge area covers the whole operating cathode area or sputter etched area in this experiment. The decrease of an electric field across both electrodes is due to an increase in current with gas temperature [5.2-5.3]. On the other hand, the positive slope is the result of the phenomenon in abnormal glow discharge region.

5.2.2 SURFACE MODIFICATION BY ARGON PLASMA

In this section, two cases which could be generated in continuous discharge mode were chosen from the V-I characteristic graphs in figure 5.2 to study surface modification due to the good stability of continuous discharge mode [5.4]. Both conditions could generate the most stable discharge, and required less I_d to sustain plasma because of higher supplied voltage compared with other conditions. From the experimental results at the same I_d of 2 μA, the first experimental condition, used 2.5 sccm GFR and 100 μm G_d, gave 840 volts of V_d, and the second experimental condition, used 5 sccm GFR and 200 μm G_d, gave 770 volts of V_d. To study the surface modification without the effect of micro arc discharge caused by thermionic electron emission due to long time gas discharge [5.5], the experiments were operated within 30 seconds before micro arc discharge initiate. Both conditions were performed in the same T_d ranging from 5, 10, 15, 20, and 30 seconds.

After igniting the stable plasma under the aforementioned conditions, the counter electrode was moved rapidly to study modification of clean surface. After 30 seconds of sputtering, sputtered surfaces on Si substrate by Argon micro plasma jet of the first and second cases are shown in figure 5.3 (a) and (b), respectively. In general, the

sputtered area diameter increases with increasing gap distance as depicted the relationship between sputtered area diameter and G_d in figure 5.4 (a).

(a)

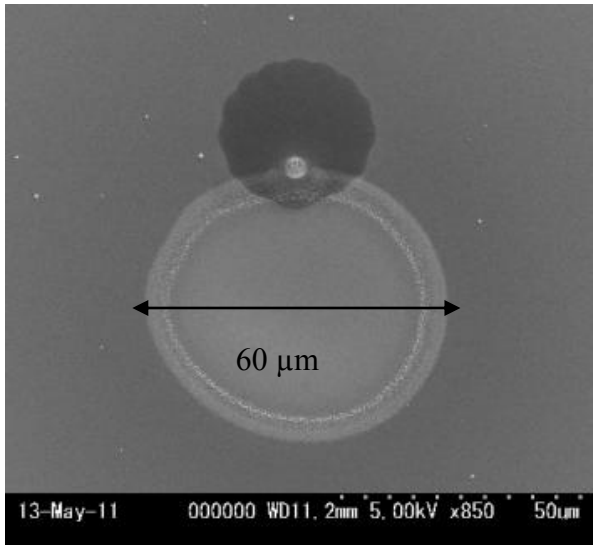

(b)

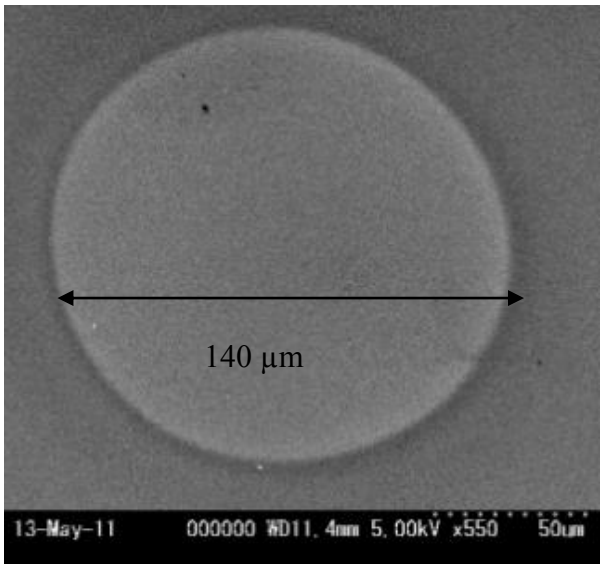

Figure 5.3 SEM images for sputtered surface on Silicon substrate by Argon micro plasma (a) using gas flow rate of 2.5 sccm and gap distance of 100 μm, (b) gas flow rate of 5 sccm and gap distance of 200 μm, at the same discharge current of 2 μA and discharge time of 30 seconds. SEM images for damages appeared in the sputtered area.

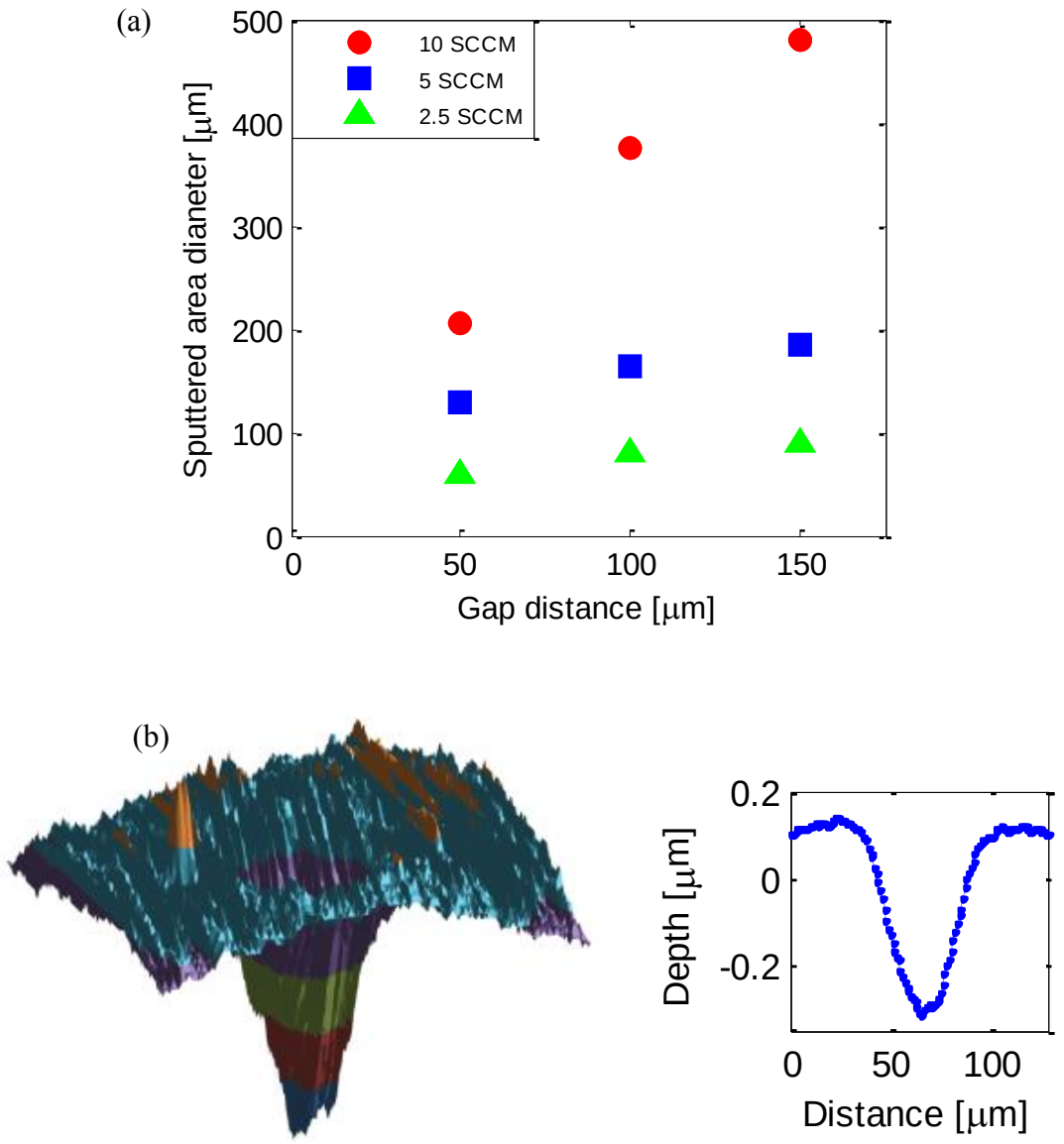

Figure 5.4 (a) The relationship between sputtered area diameter and gap distance using gas flow rate of 2.5, 5 and 10 sccm at the same discharge current of 2 μA after discharge time of 15 seconds. (b) Surface profile and its sputtered area depth profile using 2.5 sccm gas flow rate at the gap distance of 100 μm after discharge time for 30 seconds. The deepest spot was 0.31 μm and the diameter of sputtered area was 60 μm.

The shape of gas flow could be used for predicting the size of sputtered area. When the gap distance is increased, the dense gas profile reached at the irradiated area before being evacuated and bounced at the target is expanded. This reason makes sputtered area diameter increased when gap distance is increased. However, note that the larger sputtered area stated here is not implied that high sputtering rate will be obtained. The surface of sputtered area of both cases was very smooth compared to its edge where having re-deposited Si particles and dome-like structures as could be noticed in figure 5.5 (a) and (b).

Since the center of sputtered area was sputtered continuously by energetic ions, the center of sputtered area was deeper and smoother than its edge. At this sputtered edge area, it was low frequency to be sputtered because it was located far from the center of high density plasma area. Consequently, the depositions of sputtered Si particles, deposited on the edge of the sputtered area, caused the rough surface. Moreover, some of Si particles were deposited on the orifice surface, as well. In the case of 5 sccm GFR, the depth of the sputtered area was too shallow (less than 0.01 μm) to be detected by Electron beam 3-D measuring instrument (SDM-501, Sanyu electron). From the SDM-501 observation results, the surface profile and depth profile cross section of the sputtered area using 2.5 sccm GFR after 30 seconds T_d is presented in figure 5.4(b). The sputtered area shape was similar to a funnel cone having small rough surface caused by the Si depositions around the edge of sputtered area.

As discharge time (T_d) was increased, the sputtered area depth was gradually increased while the sputtered area diameter was quite constant. The deepest spot was found to be 0.31 μm depth, and the diameter of sputtered area was 60 μm. At DC power of 1.68 mW, the sputtering rate at the center of sputtered area was 0.01μm/s, which is higher than that of DC conventional sputtering. This is due to the fact that current density in the case of 2.5 sccm GFR was 70 mA/cm^2 approximately, which is 35 times higher than that of DC conventional system [5.5]. The sputtering rate of 2.5 sccm

GFR is much higher than that of 5 sccm GFR because ions in this case were accelerated by higher supplied voltage.

(a)

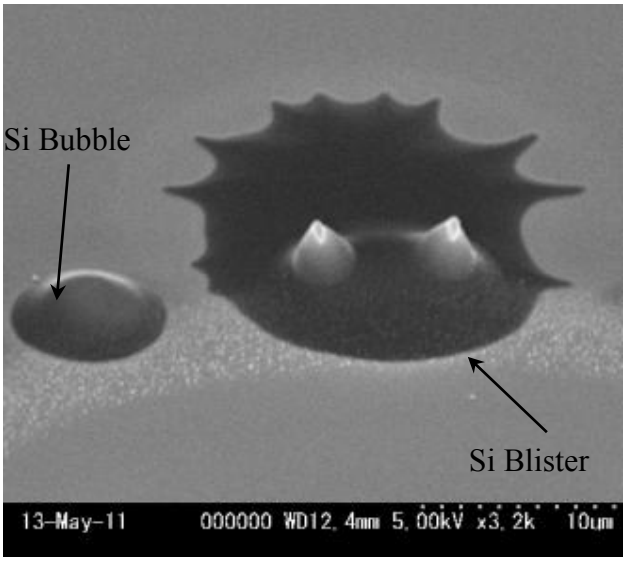

(b)

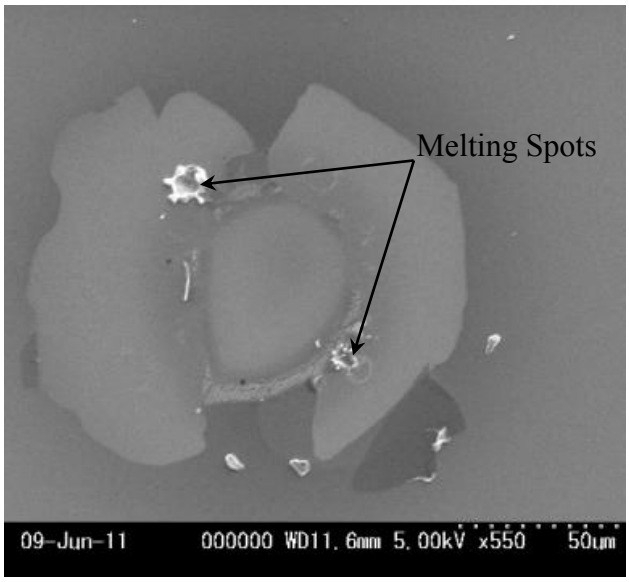

Figure 5.5 SEM images for sputtered surface on Silicon substrate by Ar micro plasma (a) silicon bubbles and blisters appeared at the edge of sputtered area, and (b) melting spots and silicon flakes caused by micro arc discharge.

In some cases, damage caused by sputtering was observed. The dome-like structure at the edge of sputtered area was confirmed the hardness by touching its surface by the needle. The dome-like structure was broken but there was no scalp bouncing off to other area. Therefore, it was named bubble due to its shape and soft surface. Figure 5.5 (a) shows SEM image for Si bubbles and blisters at the edge of sputtered area using 2.5 sccm GFR condition after T_d of 10 seconds. The bubble diameter size ranges from 0.05-5 μm in diameter. From the literature review, the bubble is formed due to knock-in of Argon gas molecule during bombardment [5.6]. If the bubble has a large of internal pressure, the bubble will be deformed and ruptured [5.7]. However, in our system, total ion energy is lower than 1 keV which is too low to cause ion implantation. Therefore, at the first step of bubble preliminary investigation, the sputtered area and bubbles were observed by Energy-dispersive X-ray spectroscopy (EDS) analysis to confirm whether there was Ar gas inside those bubbles. However, Argon element could not be detected by EDS of field emission-SEM (JEOL, JSM-7300F).

Figure 5.5(b) presents damage from the micro arc discharge [5.5] incurred during discharge. After the micro plasma was generated using 2.5 sccm GFR condition for approximately 30 seconds, arc discharge could be seen on the oscilloscope monitor monitoring the discharge current waveform. For long time plasma operation, arc discharge is initiated because high I_d can cause an increase in electrode temperature. Arc discharge occurs when the electrode temperature is high enough for thermionic electron emission [5.8]. Discharge current waveform changed from a linear line to a short pulse and then back to linear line in less than a nano second (approximately 0.55 ns) when micro arc discharge occurred. Also, the frequency of arc discharge increased when T_d increased. The number of melting spots caused by micro arc discharge is consistent with the number of observed short pulses on the oscilloscope monitor. In addition, heating from arc discharge caused Silicon peeling.

One of the problems during DC micro plasma jet generation by using orifice gas nozzle as anode is Silicon deposition on the tip of the orifice gas nozzle. Figure 5.6 shows SEM images of the orifice at the tip of gas nozzle (a) before and (b) after plasma generation. It can be seen clearly in figure 5.6(b) that there is white area, silicon deposition, around the orifice hole. This can cause an unstable discharge because Silicon deposition at the orifice obstructs the gas flow if the system is performed for long time at a short gap distance using a high, sustained discharge current.

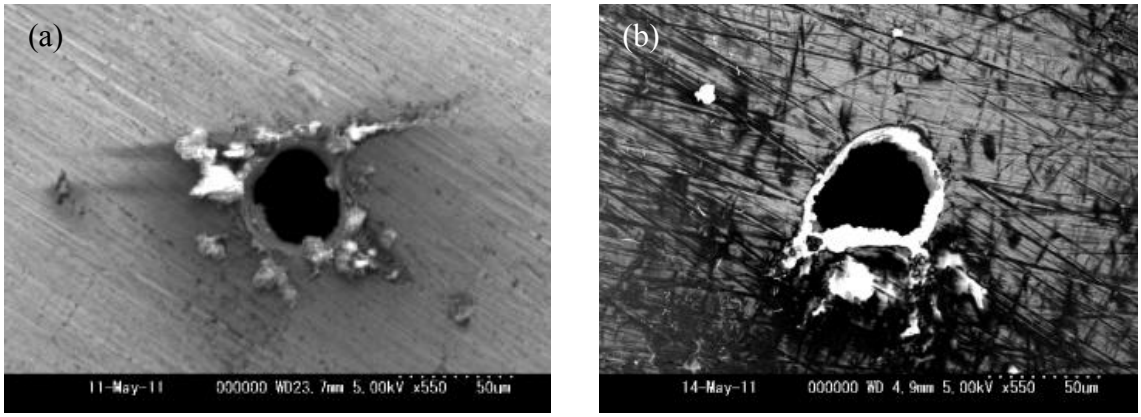

Figure 5.6 SEM images of OGN tip (a) before and (b) after plasma generation.

5.3 **SUMMARY**

Local high pressure micro plasma jet performed in SEM chamber was proposed. Small orifice gas nozzle having 40 μm in diameter was used to sputter Silicon substrate locally. Gap distance, gas flow rate and discharge parameters (I_d, V_d and T_d) playing an important role in the characteristics of local sputter etching were studied. By using Ar 2.5 sccm gas flow rate at gap distance of 100 μm, the sputtering rate of Silicon substrate was 0.01μm/s with 60 μm in diameter at DC power of 1.68 mW. The sputtered area was very smooth compared to its edge where having redeposited Si particles and bubbles.

5.4 **REFERENCES**

[5.1] Matra, K., Mitzobuchi, Y., Furuta, H. and Hatta, A. (2013). Local sputter etching by micro plasma jet in SEM. *Vacuum, 87,* 132–135.

[5.2] Shirai, N., Nakazawa, M., Ibuka, S., & Ishii, S. (2009). Atmospheric DC Glow Microplasmas Using Miniature Gas Flow And Electrolyte Cathode. *Japanese Journal of Applied Physics*, *48*(No. 3), 036002.

[5.3] Staack, D., Farouk, B., Gutsol, A., & Fridman, A. (2008). DC Normal Glow Discharges In Atmospheric Pressure Atomic And Molecular Gases. *Plasma Sources Science and Technology*, *17*(2), 025013.

[5.4] Chapman, B. N. (1980). *Glow discharge processes: sputtering and plasma etching*. New York: Wiley.

[5.5] Hirata, Y., Fukushima, M., Sano, T., Ozaki, K., Ohji, T. (2000). Micro-arc discharge phenomena. *Vacuum*. *59*, 142-151.

[5.6] Bangert, U., Goodhew, P. J., Jeynes, C., Wilson, I. H. (1986). Low-energy (2-5 keV) argon damage in silicon. *Journal of Physics D: Applied Physics. 19,* 589-603.

[5.7] Igarashi, S., Itakura, A. N., Kitajima, M., Nakano, S., Muto, S., Tanabe, T., et al. (2006). Local Oxidation Induced By Inhomogeneous Stress On Blistered Si Surface. *Japanese Journal of Applied Physics*, *45*(No. 5A), 4179-4182.

[5.8] Conrads, H. and Schmidt, M. (2000). Plasma generation and plasma source. Plasma Sources Science and Technology. 9(4), 441-454.

CHAPTER 6: LOCAL THIN-FILM DEPOSITION BY MICRO PLASMA JET IN SEM

Thin-film deposition has played a much more important role in many industrial applications such as semiconductor devices, electronic components, and tribological coating [6.1-6.3]. Among many methods for thin-film deposition—for example: chemical vapor deposition (CVD) [6.4], spin coating [6.5], and thermal evaporation [6.6]—micro plasma jet has been promoted as a special technique for micro deposition owing to its many advantages such as high plasma density, fast convection flow, miniature geometry, and flexible operation [6.7]. Micro plasma jet is hence one interesting tool for chemical deposition recently. Moreover, micro plasma jet could be also applied in surface modifications, analytical chemistry, nanostructure growth, micro chemical reactions, and biomedical treatment among others [6.1-6.3, 6.7-6.8]. In this chapter, micro plasma jet system is aimed to be applied for local thin-film deposition in SEM. The thin-film deposition and electrical discharge characteristics were studied by varying electrode gap distance, discharge current, discharge voltage, and deposition time. Furthermore, thin-film analysis was examined by in-situ SEM observation, surface profiling machine (SDM and Alpha-Step IQ), and Raman Spectroscopy for carbon composition observation.

6.1 EXPERIMENTAL PROCEDURE

The experimental set up in this chapter has been almost entirely explained in section 3.2, chapter 3. Some parameter differences were as follows: the counter electrode of OGN was placed at a gap distance (G_d) ranging from 100 to 200 μm from the OGN surface. To localize high gas density inside the vacuum system, a low OGN conductance was very essential. Therefore, the standard 1/8" SS-316 tubing closed at one end with a laser drilled hole 30 μm diameter (Lenox Laser) was chosen as OGN. The stainless steel tube was 3.05 and 3.175 mm in inner and outer diameter respectively. The OGN had conductance of 0.0825sccm/kPa, which was sufficient to confine the gas jet inside the vacuum environment. This small orifice conductance caused the pressure inside OGN

to be almost constant except at the exit of the orifice. The acetylene gas (C_2H_2) was used as a precursor gas for thin-film deposition. At 6.6 sccm C_2H_2 gas flow rate, the pressure inside OGN could be as high as 80 kPa. This is due to the large ratio of the inner diameter of main capillary tube to the orifice hole size. However, the pressure inside the OGN was changed sometimes by thin-film deposition or by electrode erosion.

6.2 EXPERIMENTAL RESULTS AND DISCUSSION

6.2.1 *VOLTAGE-CURRENT CHARACTERISTICS OF C_2H_2 DISCHARGE IN MICRO-GAS JET IN VACUUM*

After applying sufficient source voltage (*Vs*) to C_2H_2 gas jet supplied through the orifice gas nozzle, where the gap distance (G_d) to the silicon wafer had already been adjusted, C_2H_2 plasma jet could be generated. Since C_2H_2 is reactive gas and plasma is confined in very small gap distance, micro plasma jet has been significantly affected by the discharge time, which will be discussed in the later section. Therefore, to study the voltage-current characteristics of C_2H_2 discharge withholding the effect from time dependence, the square-wave pulse voltage source at 200 mHz frequency and 0.1% duty cycle was used.

Figure 6.1 shows the plots of discharge voltage and current monitored by the oscilloscope with variation of gap length (G_d) at the maximum constant gas flow rate of 6.6 sccm. At this gas flow rate, the pressure inside the OGN could be as high as 80 kPa. There were two different discharge modes that could be observed; self-pulsing mode and continuous mode, which is similar to ours and others' previous research [6.10-6.12]. These two discharge modes are separated by the minimum discharge current for sustaining continuous discharge (I_{min}), which is depicted by the short, thin vertical lines in figure 6.1. I_{min} is dependent on pressure, electrode gap distance and other parameters.

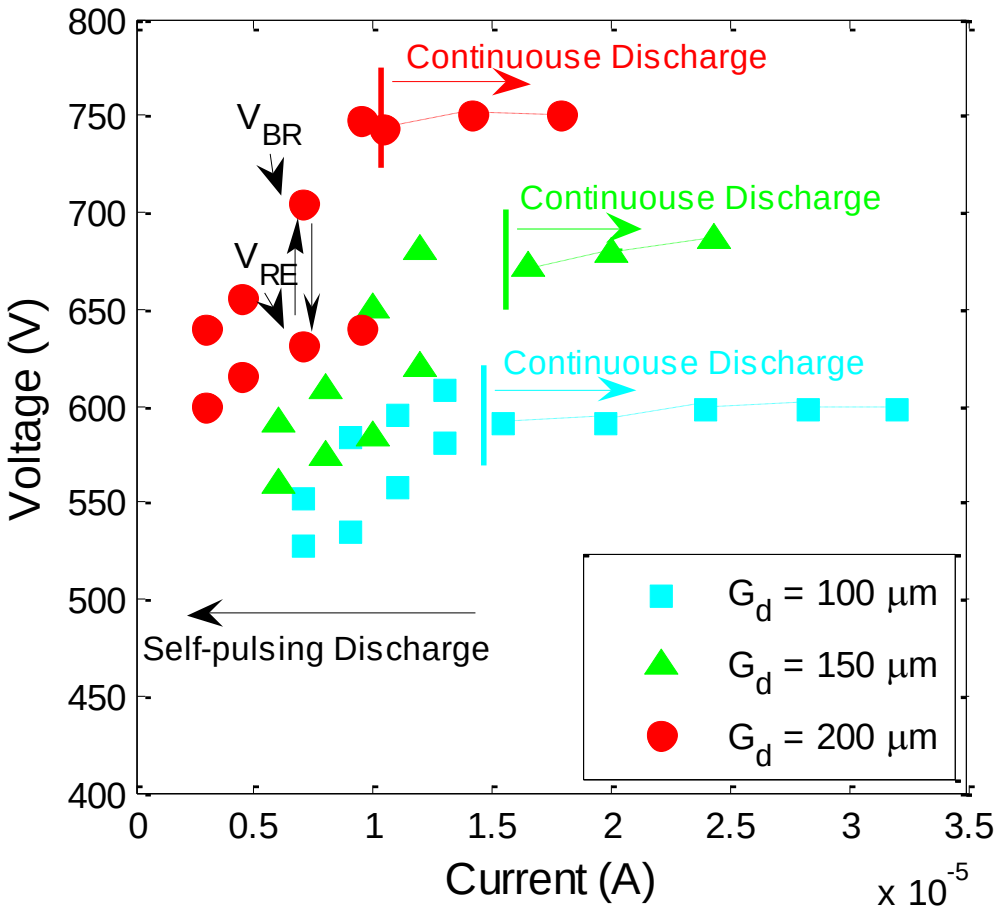

Figure 6.1 Plots of time averaged voltage and current for discharge of micro gas jet in vacuum monitored by the oscilloscope.

The self-pulsing discharge is characterized by two threshold voltages, which are recovery voltage (V_{RE}) and breakdown voltage (V_{BR}). Recovery voltage is the minimum voltage to sustain plasma, while breakdown voltage is the maximum voltage to ignite plasma [6.13]. The discharge voltage oscillates between these two voltages, and increases with the increase of average discharge current as shown in the left hand side of the short, thin vertical line in figure 6.1. The self-pulsing discharge was oscillated by the RC circuit consisting of a stray capacitor from wiring, and a large ballast resistor. During the interval of decreasing of discharge voltage, a high current peak contributed from a stray

capacitor was discharged within a few micro seconds. The detailed explanation of self-pulsing discharge had already been discussed in the chapter 4 [6.12].

Figure 6.2 shows typical waveforms of voltage and current monitored by the oscilloscope at the experimental condition of 150 μm G_d and the pressure inside the orifice of 80 kPa. The discharge at 800 V_S was automatically pulsating even if the source voltage was kept constant. The discharge at 1,000Vs was stable and continuous at the constant voltage and the constant current. In a previous work, it has been confirmed that the continuous discharge mode is suitable for local plasma processing such as micro sputter etching due to their stability [6.13].

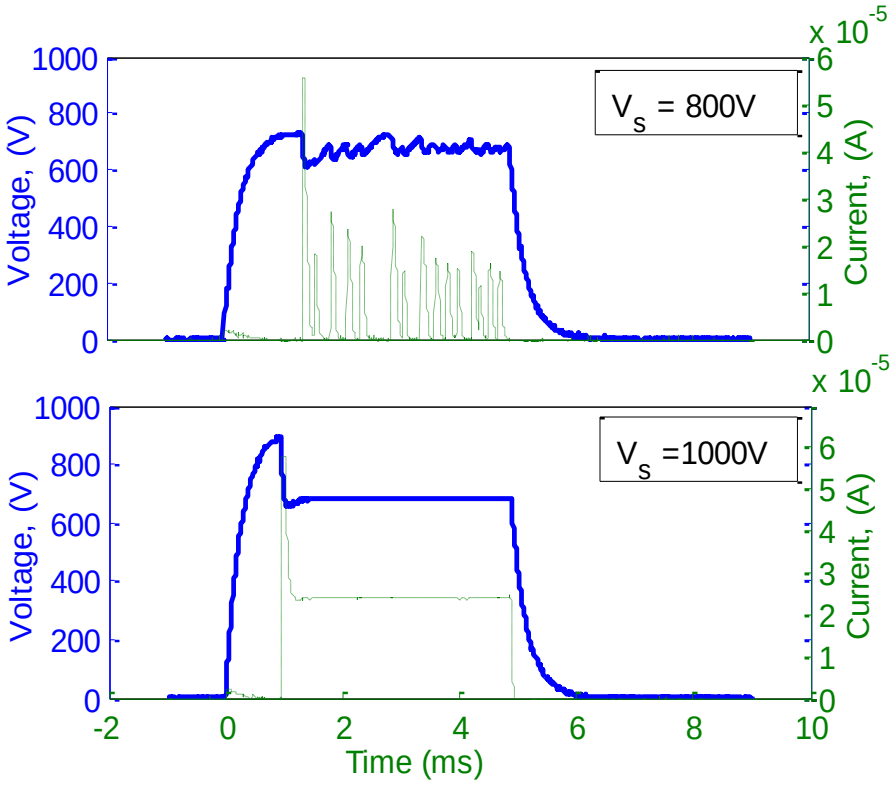

Figure 6.2 Waveforms of voltage and current monitored by the oscilloscope at 150 μm gap, 80 kPa pressure, and 800 V_S and 1,000 V_S.

By increasing the source voltage while the discharge voltage was almost constant, the discharge current limited by the ballast resistance gradually increased. The continuous discharge was observed when the current exceeded 15.5, 16 and 11 μA at the gap distance of 100, 150 and 200 μm, respectively. This is due to the fact that the current supplied from the ballast resistor was sufficiently high enough to sustain the continuous discharge ($I_d \geq I_{min}$). In this mode, discharge voltage is almost constant with variation of discharge current, which is the conventional characteristic of glow discharge.

6.2.2 *VOLTAGE AND CURRENT WITH TIME DEPENDENCE*

As mentioned in the previous section that C_2H_2 plasma is significantly affected by discharge time, the explanation of C_2H_2 plasma jet characteristic will be discussed in this section. After C_2H_2 plasma was ignited, a few seconds later, plasma was automatically stopped. Figure 6.3 shows the time average voltage-current plot of C_2H_2 plasma at the electrode gap distance of 150 μm, and at the constant applied source voltage of 1000V for 30s discharge time monitored by multi meters. At this experimental condition, C_2H_2 plasma jet was ignited at the discharge voltage of 845 V and discharge current of 24 μA. The continuous discharge could be sustained for a few milliseconds after plasma was ignited, and then turned to self-pulsing discharge. It could be noticed that the discharge voltage increased during the decreasing of discharge current when the discharge time increased. The discharge current decreased rapidly to 1.5 μA within 15s after plasma was ignited. At this point, the discharge voltage is almost constant at 955V, approximately.

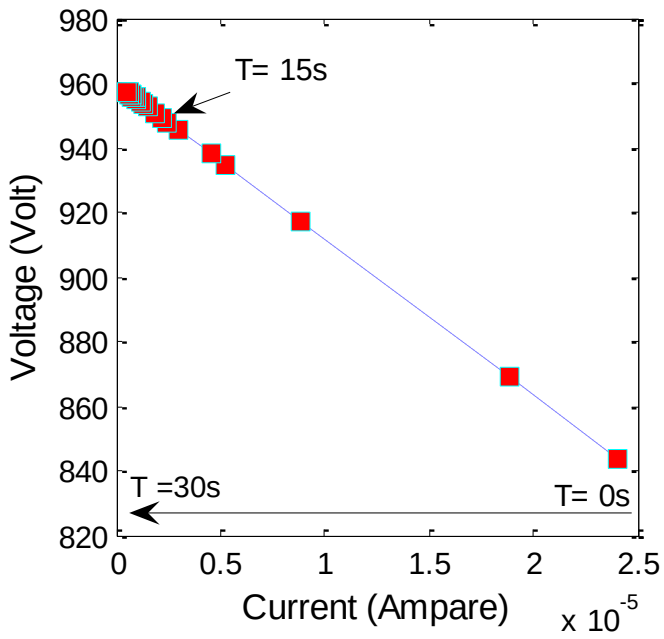

Figure 6.3 Time average voltage and current at the electrode gap distance of 150 μm and constant applied voltage of 1000V for 30s discharge time.

Figure 6.4 shows the real plot of instantaneous voltage and current of C_2H_2 plasma at the electrode gap distance of 150 μm and the constant source voltage of 1000V, at the different discharge times. The discharge current rapidly decreased with the increase of discharge voltage and discharge times. It should be noticed that the data set shown in figure 6.4 is not the same set used in figure 6.3. The slight data deviation between these two figures would come from the gap distance misalignment, or deformation of OGN during/after plasma processing. After 15 second discharge time, the discharge current was decreased to 14.4 μA, which was 3.5 times lower compared to that of 1 second discharge time. It should be emphasized that the self-pulsing discharge presented here was different from our previous research. The sustained voltages of C_2H_2 plasma were significantly increased with time compared to Argon (Ar) plasma even though the source voltage was kept constant.

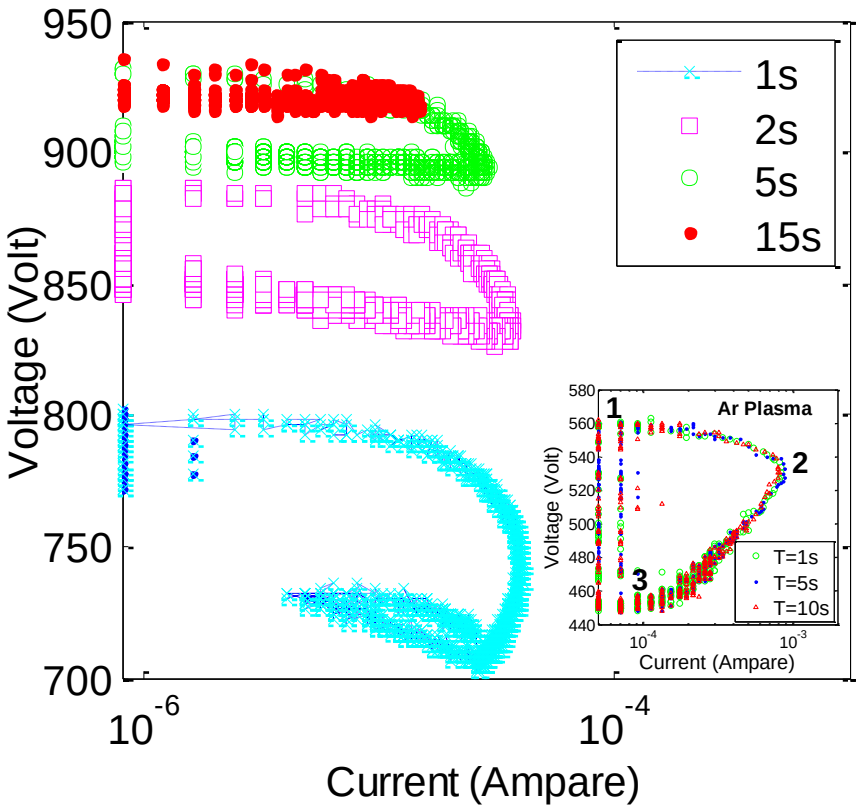

Figure 6.4 Real plots of instantaneous voltage and current for the pulsating mode monitored by the oscilloscope at 100 μm gap, 80 kPa pressure, and 1 kV_S at the different discharge times. The inset figure shows the self-pulsing of Ar plasma and current for the pulsating mode at the constant V_S at various times.

The inset figure of figure 6.4 shows the plot of voltage-current for self-pulsing mode of Ar plasma sustained by constant 900V_S at the different discharge times. The self-pulsing mode of Ar plasma could be separated into 3 phases per one cycle as explained in chapter 4. These three phases would be repeated periodically at the almost constant sustained voltages. However, in the case of C_2H_2 plasma, the self-pulsing mode could not be repeated as a cycle since the sustained voltages changed with time.

The fact which causes C_2H_2 plasma jet in our system to be extremely affected by discharge time is that the micro plasma jet was generated in the very miniature space below 200 μm. In addition, C_2H_2 plasma deposits an insulator thin-film on Si substrate with fast depositing rate. It could be confirmed that the thin-film is an insulator film since there is an electrical charge up on the thin-film during SEM observation.

An electric charge accumulated on the insulator thin-film is the number one drawback for DC gas discharge found in this research [6.14]. Insulator thin-film deposited on the silicon wafer would lessen the amount of electrons liberating from the cathode. Its surface would also accumulate positive charges. These accumulated charges would produce a high electric field, referent to the negative polarity of silicon wafer cathode; the high electric field could induce electrical breakdown and plasma termination. Moreover, local heating and arc would be possible, resulting in the film quality weakening and micro particle formation on the thin film [6.15].

After a few milliseconds of continuous C_2H_2 gas discharge, plasma could not be sustained in the continuous discharge mode as the thin-film thickness increased; it hence returned to the self-pulsing mode again before extinguishing. Increasing of insulator thin-film thickness during C_2H_2 plasma generation strongly affects the gas discharge. The insulator thin-film will not only limit the current flow by the accumulated charges on its surface, but also replace the silicon electrode by thin-film itself [6.16]. Since the conductance of insulator is much lower than that of Si wafer, the higher sustained voltages are required to sustain the plasma by the remaining electrons in the existing plasma.

However, insulator thin-film is continuously depositing on the Si cathode; therefore, the sustained voltages are practically increased with the time that the thin-film thickness has been changed. This causes the self-pulsing mode of C_2H_2 plasma jet to differ from Argon plasma jet in the previous research where the discharge voltage fluctuates between the almost constant V_{BR} and V_{RE}, and has been much influenced by the

deposition time. A possible way to overcome this problem is using pulse DC or AC power supply to reduce charge accumulation on the thin-film surface [6.7, 6.15-6.17].

6.2.3 *THIN-FILM CHARACTERISTICS*

After the C_2H_2 plasma is ignited, the thin-film deposited on the silicon cathode is the product from reactive plasma jet. The reactions at the growing film surface occur as a result of interactions between the silicon substrate and the ions, radicals, atoms, and gas molecules consisted in plasma [6.18-6.19].

(a)

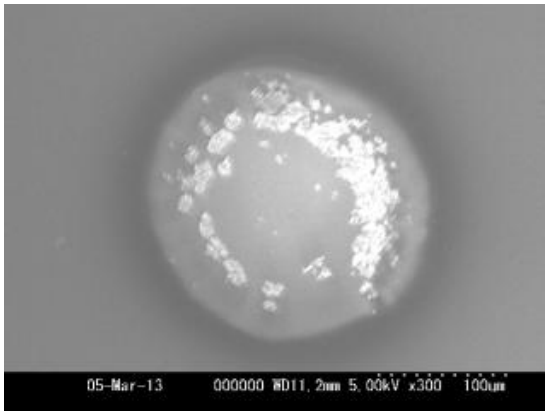

(b)

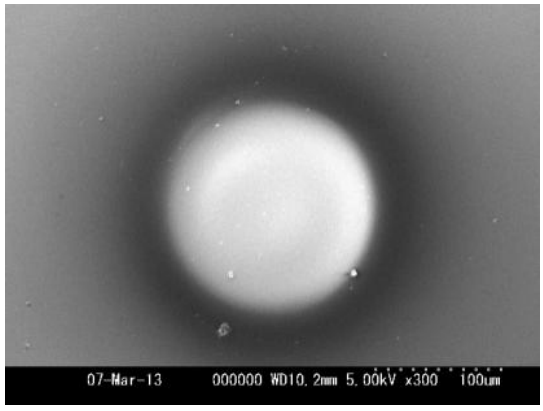

Figure 6.5 SEM image of thin-film after 5 second deposition time at 1000 kV_S and the electrode gap distance of (a) 100 and (b) 200 μm.

The experiments for thin-film deposition were conducted at the electrode gap distance of 100 and 200 μm at the same inner OGP of 80 kPa and source voltage of 1000 V. Figure 6.5a and 6.5b show the SEM image of thin-film after 5 second deposition time. The initial discharge current was about 38 and 19 μA for the 100 and 200 μm $G_{d,}$ respectively. The thin-film obtained at 100 μm G_d has a rough surface with ~~a~~ small carbon clusters having sizes ranging to 5 μm at the edge on the thin-film. Therefore, to avoid the rough thin-film surface, thin-film is deposited at the gap distance of 200 μm. However, the cause of formation of the rough surface has not been clarified yet. It would be expected that at the short gap distance, the accumulated reactive species and ion charges on thin-film have higher energy compared to that of the long gap distance at the same applied voltage. This is due to the fact that at the shorter gap distance in this experiment condition, the V_{BR} is lower than that of the longer gap distance; therefore, at the same applied source voltage, the large difference between V_{BR} and applied source voltage will contribute to accelerate charge particles inside plasma. Due to the accumulated energetic reactive species and ion charges on thin-film, the local high electric field on thin-film would lead to breakdown and formation of micro particle as could be noticed on the thin-film surface [6.15].

Figure 6.6(a) and 6.6(b) show SEM images from the top view and side view of thin-film after 15 second depositing time at G_d of 200 μm, 80 kPa OGP, and $1000V_S$. The initial discharge current was 19μA, approximately. The film is circularly-shaped with a diameter of 220 μm. It could be noticed that the thin-film shape is similar to the symmetry of a shallow mountain. The photograph of the same area taken by an optical microscope depicted in figure 6.7 could confirm that there is only one vortex at the center of thin-film. The layers of different colors at the edge of thin-film are due to the film thickness profile.

(a)

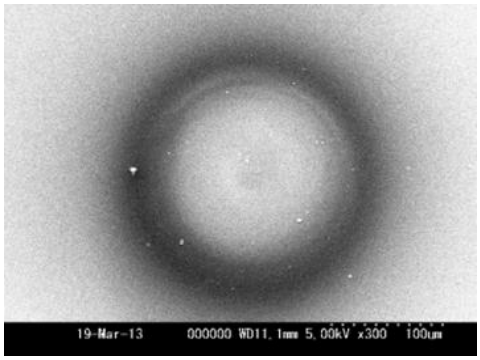

(b)

Figure 6.6 SEM image from (a) top view and (b) side view of thin-film after 15 second depositing time at the G_d of 200 µm, 80 kPa OGP, and 1000Vs.

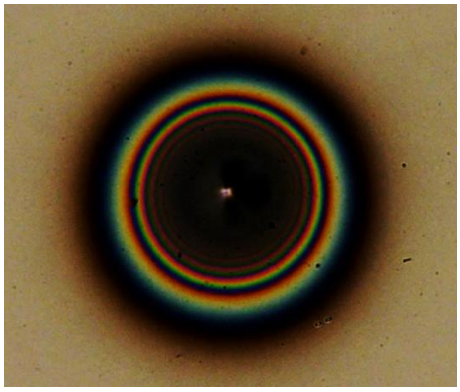

Figure 6.7 Optical photograph of thin-film after 15 second depositing time at the G_d of 200 µm, 80 kPa OGP, and 1000Vs.

Figure 6.8 shows the surface profile of thin-film after 15 seconds of discharge time at 850 and 1000 *Vs* by Alpha-step IQ. After the C_2H_2 was ignited, the initial discharge current was 13 and 19 μA for the 850 and 1000 V_S respectively. The diameter of thin-film was 175 and 220 μm at 850 and 1000 V_S respectively. The film diameter is a little larger for deposition at the higher source voltage. This is due to the smaller discharge current resulting in the smaller plasma size. The thin-film mass is practically concentrated in a single point at the center of gas flow current. From these results, it could be implied that the plasma density is nearly symmetric and thin-film thickness distribution could be fitted by Gaussian distribution. Therefore, the symmetry thin-film could be achieved by our micro gas jet model without complex design [6.20]. The smoothness and symmetry of thin-film is an advantage for good surface contact in electronic components and uniform electric field at the electrode for some applications.

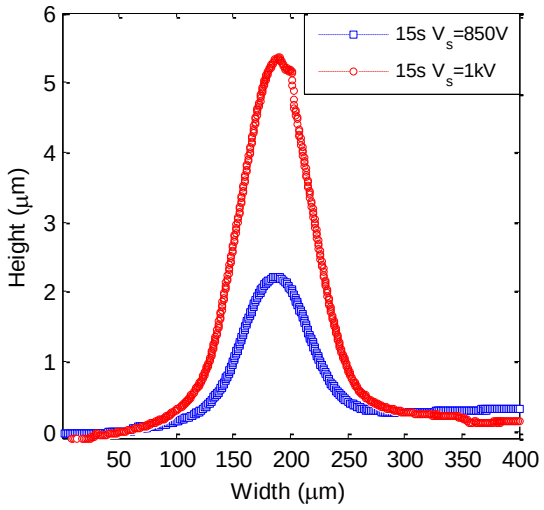

Figure 6.8 The surface profile of thin-film after 15 and 30 second C_2H_2 discharge at 850 and 1000V source voltage by Alpha-Step IQ.

The film was deposited rapidly at a few seconds after plasma was ignited. However, the film growth was almost limited in the first 15 seconds after plasma was ignited due to the accumulated charges on thin-film, as could be noticed by the nearly saturated discharge voltage in figure 6.3. Therefore, the depositing rate in this research

was calculated only for the first 15 seconds after plasma was ignited, which are 0.15 and 0.33 µm/s at 850 and 1000 V_S, respectively. This deposition rate obtained by our micro plasma jet model is higher than the conventional PECVD method by 10 times approximately [6.19].

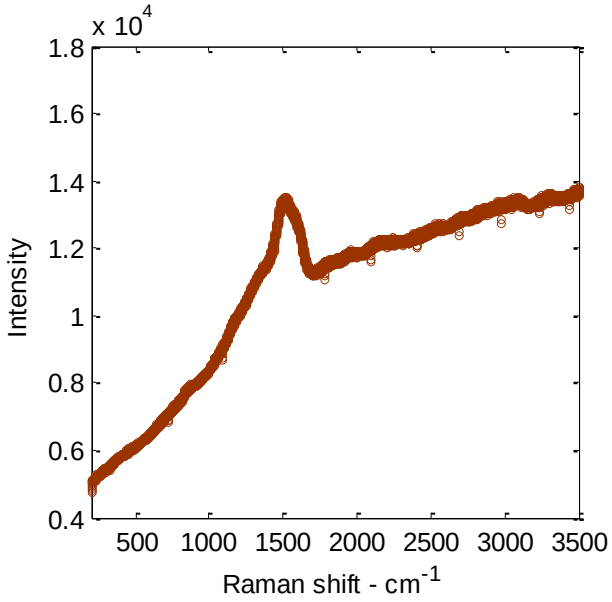

Figure 6.9 Raman spectra of the thin-film after 15 seconds at 200 G_d, 80 kPa OGP, and 1000Vs.

To characterize the thin-film, Raman spectrometer was used to analyze the thin-film. Figure 6.9 shows the raman spectra of the thin-film after 15 seconds at 200 G_d, 80 kPa OGP, and 1000V_S. The raman spectra shows the peak around 1521 cm^{-1}, which shows the property of hydrogenated amorphous carbon film (a-C:H). The film was then undergone a first preliminary hardness test by needle scratching as shown in figure 6.10. The film was stung both vertically and horizontally by a needle of 30 µm tip diameter. The film cannot be broken by stinging the needle in a vertical direction; however, when the film was scratched in a horizontal direction, it could be broken with some friction. This could be implied that the film was grown on the silicon wafer fairly firmly without

the hollow cavity under the film. Even though the presented micro plasma jet could provide a smooth, symmetrical, and hard thin-film at the local area, it still has the thin-film deposition limited to around a few 10 seconds due to increasing of insulator thin film. However, the presented micro plasma jet could deposit thin film with a fast rate which could reduce time consumption in the depositing process.

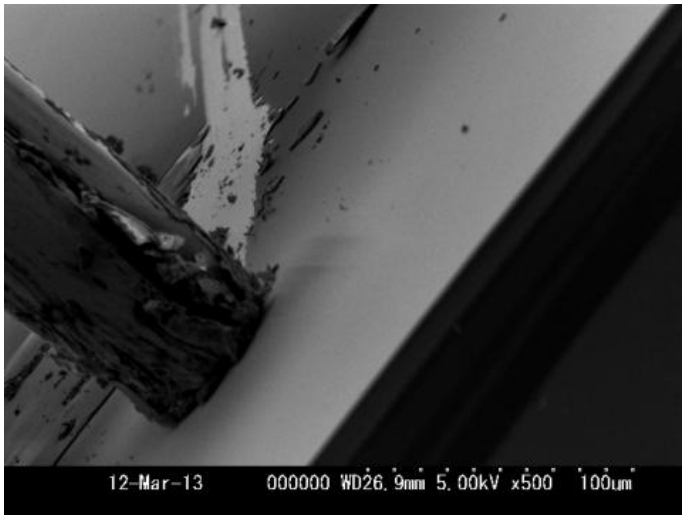

Figure 6.10 In-situ SEM image of Hardness test by needle scratching.

6.3 SUMMARY

A micro plasma jet in SEM for localized micro deposition by DC acetylene (C_2H_2) is proposed. C_2H_2 plasma jet could be confined between an orifice gas nozzle anode and Silicon counter electrode by an orifice gas nozzle. At a constant source voltage, after C_2H_2 plasma was ignited, a few seconds later, plasma was automatically stopped as a result of the deposition of insulator thin-film on Si substrate. The discharge voltage was increased during the decreasing of discharge current as the thickness of thin-film was increasing. A practically symmetrical mountain-shaped a:C-H thin-film, grown by 1kV source voltage at the gap distance of 200 μm, had a thickness of 0.35 μm after 15s deposition. At this experimental condition, the deposition rate is higher than conventional PECVD by 10 times approximately.

6.4 REFERENCES

[6.1] Ito, T., Izaki, T., & Terashima, K. (2001). Application of microscale plasma to material processing. *Thin Solid Films*,*386*(2), 300-304.

[6.2] Pothiraja, R., Bibinov, N., & Awakowicz, P. (2011). Amorphous Carbon Film Deposition On The Inner Surface Of Tubes Using Atmospheric Pressure Pulsed Filamentary Plasma Source. *Journal of Physics D: Applied Physics*, *44*(35), 355206.

[6.3] Liu, W., Guo, X., Chang, C., & Lu, J. (2009). Diamond-like Carbon Thin-films Synthesis By Low Temperature Atmospheric Pressure Plasma Method.*Thin Solid Films*, *517*(14), 4229-4232.

[6.4] Crowell, J. E. (2003). Chemical Methods of Thin-film Deposition: Chemical Vapor Deposition, Atomic Layer Deposition, And Related Technologies. *Journal of Vacuum Science & Technology A: Vacuum, Surfaces, and Films*, *21*(5), S88-95

[6.5] Hall, D. B., Underhill, P., & Torkelson, J. M. (1998). Spin Coating Of Thin And Ultrathin Polymer Films. *Polymer Engineering & Science*, *38*(12), 2039-2045.

[6.6] Sorianello, V., Colace, L., Nardone, M., & Assanto, G. (2011). Thermally Evaporated Single-crystal Germanium On Silicon. *Thin Solid Films*, *519*(22), 8037-8040.

[6.7] Benedikt, J., Focke, K., Yanguas-Gil, A., & Keudell, A. v. (2006). Atmospheric Pressure Microplasma Jet As A Depositing Tool. *Applied Physics Letters*, *89*(25), 251504.

[6.8] Mariotti, D., & Sankaran, R. M. (2010). Microplasmas For Nanomaterials Synthesis. *Journal of Physics D: Applied Physics*, *43*(32), 323001.

[6.9] Matra, K., Mitzobuchi, Y., Furuta, H. and Hatta, A. (2013). Local sputter etching by micro plasma jet in SEM. *Vacuum, 87,* 132–135.

[6.10] Shirai, N., Nakazawa, M., Ibuka, S., & Ishii, S. (2009). Atmospheric DC Glow Microplasmas Using Miniature Gas Flow And Electrolyte Cathode. *Japanese Journal of Applied Physics*, *48*(3), 036002.

[6.11] Arkhipenko, V. I., Kirillov, A. A., Safronau, Y. A., and Simonchik, L. V. (2012) DC atmospheric pressure glow microdischarges in the current range from microamps up to amperes. *The European Physical Journal,* 60(3), 455-463.

[6.12] MATRA, K., Furuta, H., & Hatta, A. (2013). Current-Voltage Characteristics of DC Discharge in Micro Gas Jet Injected into Vacuum Environment. *Journal of Physics: Conference Series*, *441*(1), 012021.

[6.13] Ovidiu. S. and STOICAN. J. (2009). Effect of an external electrode on the characteristics of a low frequency discharge.
Journal of Plasma and Fusion Research SERIE, 8, 804-808.

[6.14] Matra, K., Furuta, H. and Hatta, A. (2013). "Localized Micro Deposition by DC C_2H_2 Micro Plasma Jet in SEM", paper presented at *The 7th International Workshop on Microplasmas*, Beijing, China, 20-23 May. p. 52.

[6.15] Welzel, T. (2010). *Time-resolved characterisation of pulsed magnetron discharges for the deposition of thin-films with plasma diagnostic methods*. Ph.D. Habilitationsschrift der TU-Chemnitz.

[6.16] Belkind, A., Freilich, A., & Scholl, R. (1999). Using Pulsed Direct Current Power For Reactive Sputtering Of Al[sub 2]O[sub 3]. *Journal of Vacuum Science & Technology A: Vacuum, Surfaces, and Films*, *17*(4), 1934.

[6.17] Wachtendorf, C., Herweg, C., Daeuber, M., Benedikt, J., & Keudell, A. v. (2009). Thin-film Growth From A Low Pressure Plasma Excited In A Supersonic Expanding Gas Jet. *Journal of Physics D: Applied Physics*, *42*(9), 095205.

[6.18] Manage, D. P. (1998). *Structural and optical characterization of hydrogenated amorphous carbon thin-films.* Ph.D. University of Toronto.

[6.19] Von Keudell, A., Meier, M., & Hopf, C. (2002). Growth mechanism of amorphous hydrogenated carbon. *Diamond and related Materials*, *11*(3), 969-975.

[6.20] Benedikt, J., Raballand, V., Yanguas-Gil, A., Focke, K., & Keudell, A. v. (2007). Thin-film Deposition By Means Of Atmospheric Pressure Microplasma Jet.*Plasma Physics and Controlled Fusion*,*49*(12B), B419-B427.

CHAPTER 7: CONCLUSIONS

Characteristics of micro plasma jets operated in a micro gas jet injected into a vacuum environment was clarified by using an orifice of a few tens of μm diameters as an anode and the Si substrate for cathode equipped in SEM chamber. The discharge showed a self-pulsing mode and a continuous mode. The continuous discharge mode occurred at a lower gas jet pressure with a longer gap distance at larger current. The self-pulsating of the voltage and current was investigated using a discharge circuit model which included a stray capacitor.

The DC micro plasma jet was subsequently applied to micro plasma processing. In the first application, local sputter etching by argon plasma jet was proposed. A small orifice gas nozzle, 40 μm in diameter, was used to locally sputter a Silicon substrate. By using Argon 2.5 sccm gas flow rate at an electrode gap distance of 100 μm, the sputtering rate of the Silicon substrate was 0.01μm/s with 60 μm in diameter at a DC power of 1.68 mW. The sputtered area was very smooth compared to its edge, which had bubbles and redeposited Si particles.

The second application was a local thin-film deposition by a C_2H_2 plasma jet. The C_2H_2 plasma could be confined between an orifice gas nozzle anode and a Silicon counter electrode. At the constant applied source voltage, after C_2H_2 plasma was ignited, a few second later, the plasma was automatically stopped as a result of the deposition of insulator thin-film on Si substrate. The discharge voltage increased during the decreasing of discharge current as the thickness of thin-film was increasing. A practically symmetrical bell shape a:C-H thin-film, grown by 1kV_S at the gap distance of 200 μm with the initial discharge current of 19 μA, had a thickness of 5 μm after 15s deposition. In this experimental condition, the deposition rate was 0.33μm/s, which was approximately 10 times higher than conventional PECVD. However, plasma could not be

sustained for a long time for thin-film deposition due to the increasing of thin-film insulator covering on the cathode surface.

LIST OF PUBLICATIONS

INTERNATIONAL JOURNAL PAPERS

[1] MATRA, K., Furuta, H., & Hatta, A. (2013). Current-Voltage Characteristics of DC Discharge in Micro Gas Jet Injected into Vacuum Environment. *Journal of Physics: Conference Series*, *441*(1), 012021.

[2] Matra, K., Mitzobuchi, Y., Furuta, H. and Hatta, A. (2013). Local sputter etching by micro plasma jet in SEM. *Vacuum, 87,* 132–135.

INTERNATIONAL CONFERENCES

[3] Hatta, A., Mori, Y., Matra, K., Oh, J. and Furuta, H. (2013). "Microplasma jet in SEM", paper presented at *The XXXI edition of the International Conference on Phenomena in Ionized Gases (ICPIG)*, Granada, Spain, 14-19 July.

[4] Matra, K., Furuta, H. and Hatta, A. (2013). "Localized Micro Deposition by DC C2H2 Micro Plasma Jet in SEM", paper presented at *The 7th International Workshop on Microplasmas*, Beijing, China, 20-23 May. p. 52.

[5] Matra, K., Furuta, H. and Hatta, A. (2012). "Characteristics of DC Micro Plasma Jet in Vacuum", paper presented at *11th Asia-Pacific Conference on Plasma Science and Technology (APCPST-11) and 25th Symposium on Plasma Science for Materials (SPSM-25)*, Kyoto, Japan, 2–5 October. p. 131.

[6] Matra, K. and Hatta, A. (2011). "Micro Plasma Sputtering in SEM", paper presented at *The 4th Thailand-Japan International Academic Conference*, Tokyo, Japan, 26-27 November. p. 40.

[7] Matra, K., Mitzobuchi, Y., Furuta, H. and Hatta, A. (2011). "Local sputtering by micro plasma jet in SEM", paper presented at *11th international symposium on Sputtering & Plasma Process*, Kyoto, Japan, 6–8 July. p.46.

DOMESTIC CONFERENCE

[8] Matra, K., Furuta, H. and Hatta, A. (2011). "Micro Silicon Bubble Formation during Argon Micro Sputtering in SEM", paper presented at *Plasma Conference 2011*, Kanazawa, Japan, 22-25 November.